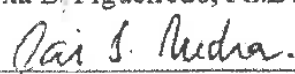The Dissertation Committee for Norah Abdullah Albekairi certifies that this is the

approved version of the following dissertation:

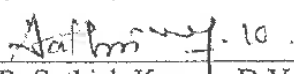# Folate Receptor-Targeted Transplacental Delivery of Digoxin for the Treatment of Fetal Arrhythmia

Committee:

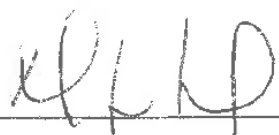_Erik Rytting_

Erik Rytting, Ph.D., Mentor

Marxa L. Figueiredo

Marxa L. Figueiredo, Ph.D.

Jai S. Rudra

Jai S. Rudra, Ph.D.

Sathish Kumar

K. R. Sathish Kumar, D.V.M., Ph.D.

David W. Niesel

David W. Niesel, Ph.D.

Dean, Graduate School

Folate Receptor-Targeted Transplacental Delivery of Digoxin for the Treatment of Fetal Arrhythmia

by

Norah Abdullah Albekairi, B. Pharm.

Dissertation

Presented to the Faculty of the Graduate School of

The University of Texas Medical Branch

in Partial Fulfillment

of the Requirements

for the Degree of

Doctor of Philosophy in Biomedical Sciences

Department of Pharmacology and Toxicology

The University of Texas Medical Branch

June, 2015

Dedication

This dissertation is dedicated to my beloved father, Professor Abdullah Mohammed Albekairi, who inspired me to pursue a doctoral degree and an academic career.

Acknowledgements

Folate Receptor-Targeted Transplacental Delivery of Digoxin for the Treatment of Fetal Arrhythmia

Publication No._____

Norah Abdullah Albekairi, seeking Ph.D.

The University of Texas Medical Branch, 2015

Supervisor: Erik Rytting

Fetal tachyarrhythmias is one of the leading causes of fetal hydrops and, ultimately, fetal demise. This condition is typically treated with transplacental digoxin by maternal administration. However, maternal digoxin administration is associated with nausea, vomiting, heart block and sinus bradycardia. Additionally, placental efflux mechanisms limit the transfer of digoxin to the fetus. When transplacental digoxin therapy fails, direct fetal injection of digoxin is performed. This can result in fetal injury, infection, and in severe cases, fetal demise. The purpose of this project is to develop a novel therapeutic strategy using nanoparticles targeting the placenta to increase digoxin delivery to the fetus. Biocompatible digoxin-loaded polymeric nanoparticles were prepared and their physicochemical and drug release characteristics were determined. Using BeWo (choriocarcinoma) cells as an *in vitro* transplacental transport model, we were able to show that these nanoparticles increase permeability of digoxin across the placenta by evading placental efflux. Conjugation of folic acid to the surface of these nanoparticles increased the transplacental transfer of digoxin due to folate receptor-mediated endocytosis. Folate receptors are highly expressed in the placental trophoblast throughout pregnancy due to the importance of folic acid in fetal and placental

development. We believe that this novel treatment strategy may increase the transfer of digoxin to the fetus and ultimately reduce maternal side effects and the need for direct fetal digoxin administration. This should result in better maternal and fetal outcomes in cases of fetal tachyarrhythmia.

TABLE OF CONTENTS

List of Tables

List of Figures

List of Abbreviations

ADP	Adenosine diphosphate
ATP	Adenosine triphosphate
BCRP	Breast cancer resistance protein
CV	Coefficient of variation
DCC	Dicyclohexylcarbodiimide
DMEM	Dulbecco's modified Eagle's medium
DSC	Differential scanning calorimetry
EDAC	1-ethyl-3-(3-dimethylaminopropyl)carbodiimide
FA	Folic acid
GPC	Gel permeation chromatography
hCG	Human chorionic gonadotropin
HPLC	High performance liquid chromatography
MES	2-(N-morpholinoethane)sulfonic acid
M_n	Number average molecular weight
M_p	Peak average molecular weight
mRNA	Messenger ribonucleic acid
MRP1	Multi-drug resistance protein 1
mV	Millivolts
MWCO	Molecular weight cut-off
NHS	N-hydroxysuccinimide
PDA	Photodiode array detector
PDI	Polydispersity index

P_e	Apparent permeability
PEG	Polyethylene glycol
P-gp	P-glycoprotein
PLGA	Poly(lactic-*co*-glycolic acid)
rpm	Revolutions per minute
SVT	Supraventricular tachycardia
TEER	Transepithelial electrical resistance
THF	Tetrahydrofuran
WST	Water soluble tetrazolium

Chapter 1: Introduction

This dissertation project is focused on the development of a novel treatment strategy for fetal arrhythmia. The document is divided into five chapters. Chapters 1 and 5 are the introduction and conclusion chapters, respectively. Chapters 2, 3, and 4 describe the three major aims of the project. Each chapter includes the proposed experiments, the results of those experiments, and conclusions, along with tie-ins to the subsequent chapters and the overall project. In the introduction, background information regarding pregnancy, fetal arrhythmia, and nanotechnology are discussed.

FETAL CONGESTIVE HEART FAILURE AND FETAL ARRHYTHMIA

Fetal congestive heart failure is defined as the failure of the developing fetal heart to adequately pump fetal blood, failing to meet the circulatory needs of the fetus. This typically results in an effusion, which is a collection of fluid in fetal compartments. These can have many potential causes, including Parvovirus B19 infection, anemia, congenital heart disease (e.g. incompetent heart valves), twin-twin transfusion, or fetal arrhythmias [1].

Fetal arrhythmias can occur in 1-2% of all pregnancies [2]. Though the embryonic heart begins beating at 3 weeks [3] and sinus rhythm begins at 9-10 weeks, fetal arrhythmias are only detected late in pregnancy. Because of this late detection, diagnosis may be delayed even into the third trimester [4]. Arrhythmias are divided into two categories: tachyarrythmias, or those with increased heart rates compared to normal, and bradyarrythmias, or those with decreased heart rates. The majority of fetal arrhythmias are tachyarrhythmias (defined as a fetal heart rate of 220 to 260 beats per minute) and are typically supraventricular, i.e., originating superior to the heart's ventricles [4]. These

types of arrhythmias occur in 0.4-0.6% of all pregnancies. Bradyarrhythmias (less than 110 beats per minute) are also possible in the fetus, and are associated with heart block, i.e., slowed or stopped conduction between the atria and the ventricles [3]. Fetal tachyarrythmia is usually diagnosed by echocardiography, though the timing of the diagnosis often depends on gestational age and other complicating factors [5]. Fetal supraventricular tachyarrhythmia (SVT) accounts for more than 50% of clinically significant fetal arrhythmias [3].

Unfortunately, many cases of fetal arrhythmia and fetal congestive heart failure as a whole can lead to a deadly condition known as *hydrops fetalis* [6]. *Hydrops fetalis* is characterized as a condition in which effusions occur in two or more fetal compartments. Effusions can occur in the lungs, peritoneal cavity, or other soft tissue [7]. *Hydrops fetalis* is often characterized as immune or non-immune , with immune being related to Rh incompatibility between the mother and the fetus. Fetal hydrops is associated with up to 72% fetal mortality [6,8]. This lethal condition occurs in one of every 2500 to 3000 pregnancies. Ultrasound is highly sensitive in the detection of *hydrops fetalis*, though other diagnostic modalities are essential in elucidating the cause [7].

CURRENT TREATMENT OPTIONS

If treated, fetal tachyarrhythmia will not necessarily lead to *hydrops fetalis*. There are a few first-line treatment options for fetal tachyarrythmia, including sotalol, flecainide, and digoxin [4,9,10]. Digoxin is most commonly used, though it can be paired with either sotalol or flecainide, if the arrhythmia is refractory to single drug therapy [3,9]. Digoxin has utility in many types of tachyarrhythmia, therefore, it is often used as a first line treatment for atrial ectopic tachycardia, multifocal atrial tachycardia, and reentrant supraventricular tachycardia [4]. Maternal plasma concentrations of all of these drugs can be monitored to approximate the fetal dose. Transplacental therapy, i.e. maternal

administration for delivery across the placenta to the fetus, is typically used until arrhythmias become refractory to these, in which case more direct measures are employed (see *Introduction: Current routes of fetal administration*).

DIGOXIN

Digoxin is a cardiac glycoside, derived from the foxglove plant [11]. In general, cardiac glycosides are composed of a steroid nucleus, namely a four-ringed structure (**Figure 1.1**). Carbon 17 of this structure is attached to an unsaturated 5 member lactone ring, and carbon three is bound to a chain of 3 sugar molecules. Typically, for digoxin and its derivatives, pharmacokinetics are dictated by the steroid nucleus, while potency is typically governed by the number of sugar molecules attached to carbon 3. Digoxin exhibits no net charge, and has an octanol water partition coefficient, or Log(D), of 1.4 at physiological pH, making it a fairly lipophilic molecule [12]. Typically, it distributes within peripheral tissues. It is approximately 37% protein bound in plasma, and is a well known substrate of P-glycoprotein (an efflux protein present in many epithelial barriers, including the placenta). Though it is typically cleared by excretion via the kidneys, 30% of elimination is via hepatic metabolism [11,12].

Digoxin, like other cardiac glycosides, functions by inhibiting the Na^+/K^+ ATPase [13]. This pump is typically responsible for maintaining the gradient of potassium and sodium across cellular membrane, which in cardiac myocytes allows for the generation of action potentials. Intracellular calcium is exchanged for sodium across the membrane by a Na^+/Ca^{2+} exchanger. When the Na^+/K^+ ATPase is blocked, intracellular calcium concentrations are elevated [14]. Intracellular calcium is responsible for the contractility of cardiac myocytes, and increases in intracellular calcium cause increased contractility of the heart, a phenomenon known as positive inotropy (**Figure 1.2**). Aside from this

3

mechanism, digoxin is a negative chronotrope (i.e. decreasing heart rate) and negative dromotrope (i.e. decreasing conduction velocity) by stimulation of the Vagus nerve [15].
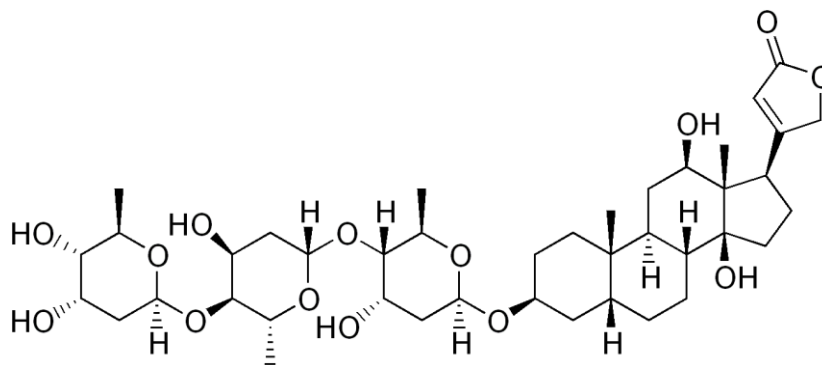
Figure 1.1. Structure of digoxin.

Digoxin is composed of a steroid nucleus with an unsaturated lactone ring on carbon 17 and a sugar moiety on carbon 3 [11].

Interestingly, the use of digoxin in the treatment of fetal tachyarrhythmia becomes more important when tachyarrhythmia leads to acute fetal congestive heart failure; because in these settings, digoxin is able to rapidly restore sinus rhythm and can be used for immediate and long-term therapy [3].

Maternal toxicity is the most serious issue when administering digoxin for the treatment of fetal heart disease. Side effects include nausea, vomiting, and altered color vision [13]. Additionally, digoxin can actually be proarrhythmic, commonly causing sinus bradycardia and heart block (i.e., slowed or ceased conduction across the atrioventricular node). This dangerous and potentially fatal toxicity profile is seen because of the high

levels of digoxin administered to the mother in order to reach the required fetal concentrations [4,16–18].
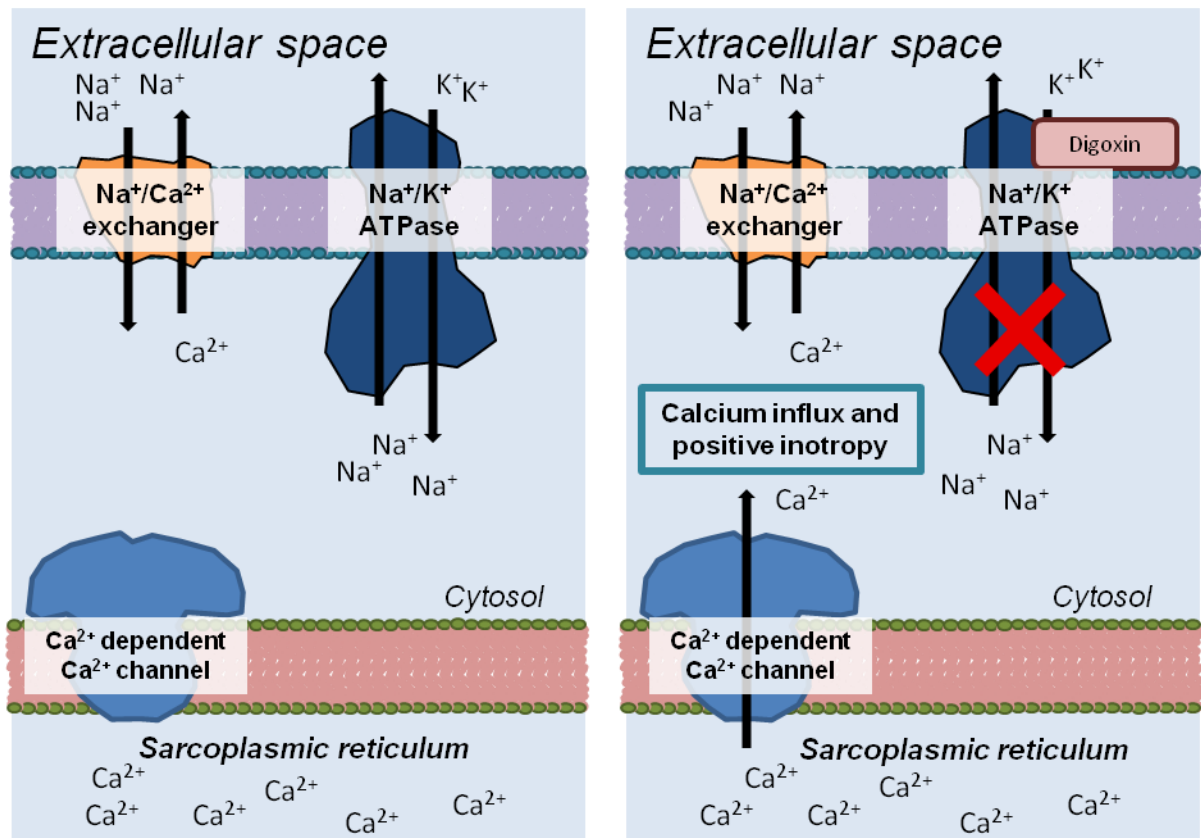
Figure 1.2. Mechanism of action of digoxin in cardiomyocyte.

Digoxin binds the Na^+/K^+ ATPase, causing influx of calcium and an increase in contractility of the cardiac myocytes (positive inotropy). Calcium dependent calcium channel allows calcium-dependent calcium influx from sarcoplasmic reticulum [13,15].

CURRENT ROUTES OF FETAL ADMINISTRATION OF DIGOXIN

There are currently two main routes of fetal administration, maternal administration for transplacental transfer or direct fetal injection. The first choice is maternal administration, which can be either oral or intravenous. Digoxin is orally bioavailable, though absorption varies between patients [11,12,19]. Monitoring of maternal plasma concentration is necessary in order to prevent maternal overdose while allowing sufficient fetal delivery, a delicate balance that can be difficult to maintain [16]. Digoxin monotherapy, either oral or intravenous, is typically attempted before multi-drug therapy is used.

When fetal arrhythmia is refractory to multi-drug transplacental therapy, direct fetal injection is attempted [3]. Modes of direct fetal pharmacotherapy include intramuscular, intracordal, intraperitoneal, and even intracardiac injections [5]. These are much more dangerous procedures, because of the precision required and movement of the fetus *in utero*. Small errors can cause severe problems, including neurovascular injury (specifically sciatic nerve injury in the case of intramuscular injection into the buttocks), skin laceration [4,5,17], and infection [20,21]. In some cases, direct fetal injection can cause fetal demise [17]. Thus, this treatment strategy is typically reserved for severe cases [3].

DIGOXIN PHARMACOKINETICS

The reasons for the severe toxicities associated with digoxin administration have to do with both the narrow therapeutic window of digoxin [18], as well as alterations in the pharmacokinetics of digoxin during pregnancy (**Table 1.1**) [12]. Since digoxin is primarily renally excreted, an increase in the renal clearance of digoxin results in a shortened elimination half-life [22]. Additionally, the volume of distribution of digoxin is increased

6

in pregnancy [12]. Plasma protein binding may be affected by reduced plasma protein concentration during pregnancy [22].

Table 1.1. Pharmacokinetics of digoxin in the non-pregnant adult vs. the pregnant patient.

	Non-pregnant	**Pregnant**	**Source(s)**
Elimination half-life	46.5 ± 16.4 hours	38.4 ± 8.7 hours	[23]
Renal clearance	115 ± 25 ml/min	181 ± 25 ml/min	[23]
Volume of distribution	7 L/kg	5.7 L/kg	[16]
Percent unbound	63 ± 5 %	67 ± 4 %	[23]

Table 1.2. Loading and maintenance doses of digoxin.

Dosing in non-pregnant adults for the treatment of supraventricular tachycardia vs. the dosing in pregnant patients treatment of fetal supraventricular tachycardia [15,23,24].

	Supraventricular tachycardia	**Fetal supraventricular tachycardia**
Loading dose	0.5-0.75 mg/24 hr PO	1.2-1.5 mg/24 hr IV
Maintenance dose	125-375 µg/24 hr PO	375-750 µg/24 hr PO
Plasma concentration	1.5 ng/mL	0.7-2.0 ng/mL

Because of the activity of P-glycoprotein in the placenta, dosing of digoxin for the treatment of fetal tachyarrhythmia is different than digoxin dosing for the treatment of tachyarrhythmias in the adult (**Table 1.2**). Increased loading doses and maintenance doses while treating fetal arrhythmia are required to elevate the plasma concentration sufficiently to achieve adequate fetal digoxin delivery. These elevated plasma concentrations bring the mother closer to toxic levels and levels that can cause fatal overdose.

PLACENTA

The human placenta is the functional barrier between the mother and the fetus during pregnancy. A tissue of fetal origin the placenta is composed of intricate villous structures housed within placental cotyledons (**Figure 1.3**) [17]. Within the villous trees of the placenta are fetal capillaries, which carry blood in close proximity to the maternal circulation, which bathes the outsides of the villous trees. Though not directly connected, maternal and fetal circulations can pass nutrients, hormones, and metabolites between one another across a cellular layer known as the placental trophoblast [25]. The placental trophoblast is an epithelial barrier between the maternal and fetal circulations that acts as the rate limiting barrier for drugs and xenobiotics passing between the maternal circulation and fetal circulations [26]. A number of mechanisms are in place to ensure that the right nutrients can pass to the fetus, while limiting the transfer of other, potentially harmful compounds to the fetus [25].
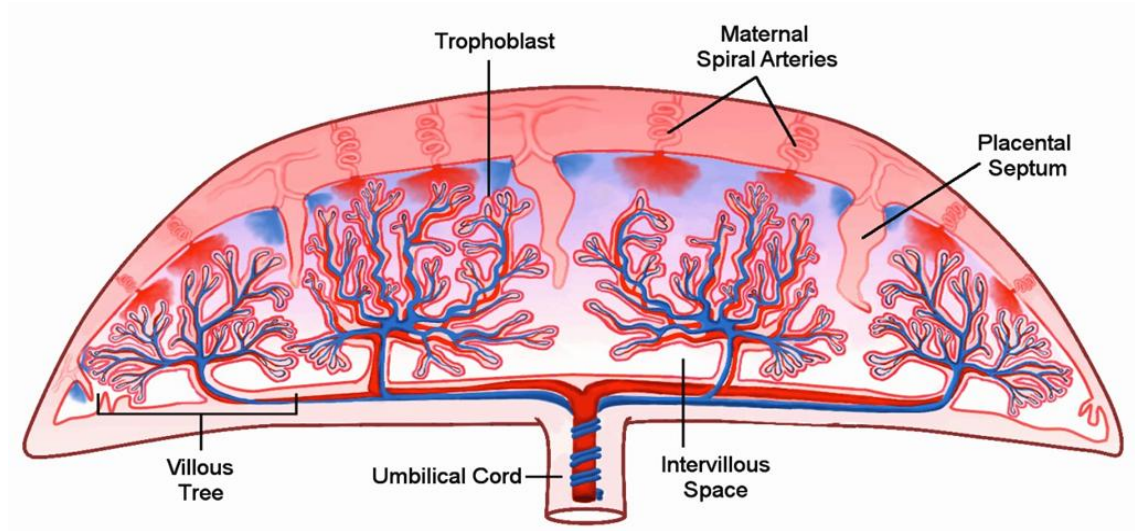
Figure 1.3. Placental morphology.

The placenta is composed of villous trees that are bathed in maternal blood. The barrier between the maternal and fetal circulations is the placental trophoblast [17].

The placental trophoblast is a group of cells that originate from the developing embryo. During implantation, this layer invades the uterine epithelium and stroma of the mother, and then differentiates into two cell types known as the cytotrophoblast and syncytiotrophoblast [27]. Villous trees form within these layers from these two cell types, with the syncytiotrophoblast in direct contact with the maternal circulation and the cytotrophoblast making up the inner bulk of the villi. Eventually, this two-celled barrier becomes thinner as the mesodermal core and fetal capillaries enter the villous structure [25–27].

Hormone production is one of the chief functions of the placenta. These include polypeptide hormones such as human chorionic gonadotropin (hCG), commonly used in the detection of pregnancy by home pregnancy tests, and steroid hormones such as progesterone and estrogens (estradiol and estriol) [28,29].

As described above, one of the chief functions of the placental trophoblast is the barrier it provides towards compounds entering the fetal circulation from the maternal circulation. This is achieved by metabolism of compounds by enzymes, as well as efflux proteins that actively pump compounds back into the maternal circulation. Many of the metabolic enzymes that are found in the placenta are also found in the adult liver, although the expression and activity of these enzymes may be different [17]. Efflux is made possible by a host of efflux transporters present on the apical surface of the placental trophoblast. These proteins utilize energy to actively pump compounds that enter the trophoblast apical membrane or cytosol back into the maternal circulation. Examples of these include P-glycoprotein (P-gp), breast cancer resistance protein (BRCP), and multidrug resistance-associated protein 1 (MRP1) [30]. These proteins are somewhat redundant in their substrate specificity, and this factor plus variable expression/activity between patients can cause differences in the amount of drug received by the fetal compartment [17,31].
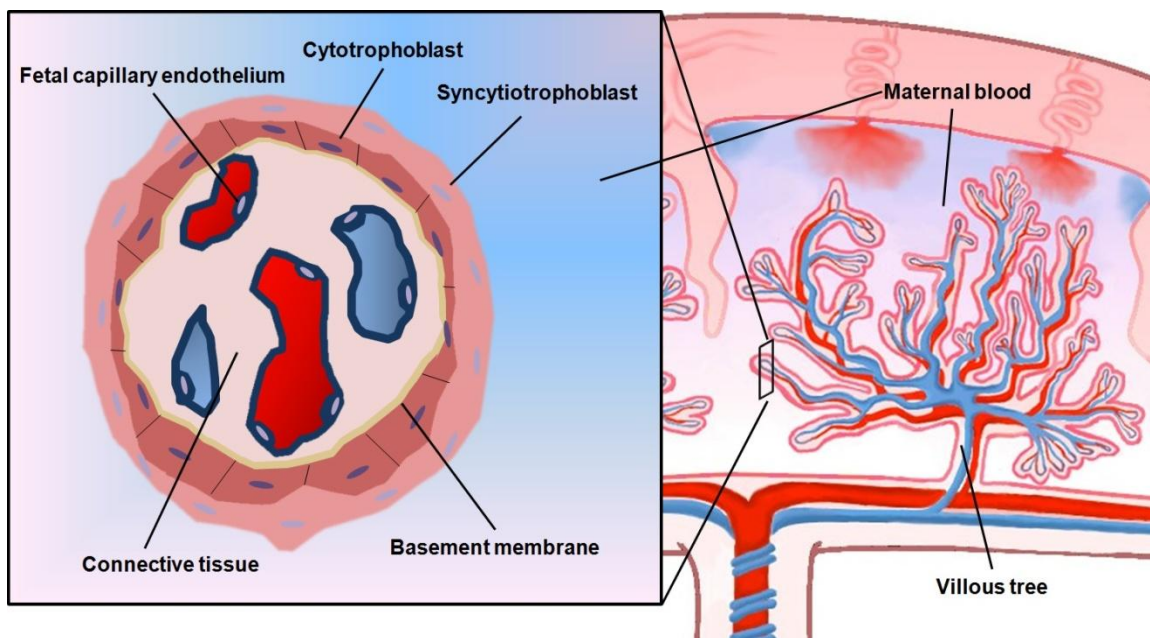
Figure 1.4. Chorionic villi (right) and cross section of chorionic villus (left).

Maternal blood flows on the outside of the villi, while fetal blood courses through the capillaries. The layers between the maternal and fetal blood are the placental trophoblast, the villous stroma, and the fetal capillary endothelium.

Digoxin is a well known substrate of P-gp and is therefore subject to the differences in expression levels and activity of the protein found between patients. P-gp, in particular, is one of the primary causes of maternal toxicity during fetal digoxin therapy; efflux of digoxin from the placenta causes higher maternal plasma concentrations than in the fetal circulation. High maternal plasma levels are required to treat fetal arrhythmias, and still some arrhythmias may be refractory to digoxin and multidrug therapy [3].

PROJECT OVERVIEW

Summary of current treatment strategies for fetal arrhythmia

As discussed above, current treatment strategies for fetal arrhythmia are suboptimal at best. Aside from maternal toxicity due to high plasma digoxin levels, desperate situations calling for direct fetal injection can cause fetal morbidity and mortality. The main reasons for these issues are that systemic delivery of digoxin inevitably causes the mother to receive part of the dose, and that P-gp efflux decreases the amount of drug that passes to the fetus. P-gp efflux in particular, increases the required loading and maintenance doses in order to achieve a therapeutic level in the fetus. All of these result in poor fetal dosing, severe maternal side effects, and the potential need for multidrug therapy and direct fetal injections.

Nanotechnology

The problems associated with digoxin administration for the treatment of fetal tachyarrhythmia may be overcome by using nanoparticles as a drug delivery vehicle. Nanoparticles are defined as particles that are on the nanometer scale, typically below 1 micron in diameter [32]. They are unique in that the physical and chemical properties of nanoparticles are, in some cases, vastly different from the materials they are derived from. These properties, as well as their size, make them desirable for certain applications where traditional materials may fall short. They also have high surface-to-mass ratios [32,33].

Nanoparticles are already present in many consumer products. The types of nanoparticles in these products include silver (primarily used for its pesticide and antimicrobial functions), titanium (primarily present in sunscreens and as a food

additive), and carbon fullerenes (carbon structures with unique electron orbital properties that grant them utility in batteries, electrodes, and solar cells) [33,34]. The presence of nanoparticles in these products gives them many desirable characteristics, but some of their properties also increase their potential for toxicity [33,35,36].

The behavior of nanoparticles in biological contexts may be different than that of their parent materials. Though small molecules are generally able to physically cross biological barriers, nanoparticles may also traverse these barriers, including epithelial barriers, and may cause increased toxicity or other changes in cellular function [35]. Additionally, they may biodistribute in certain organs based on their physicochemical properties. For instance, some particles may enter the central nervous system, and many are likely to accumulate in the liver and spleen. In some cases they can cause tissue damage [36]. Thus, it is important to understand the specific properties of the nanoparticles in question by use of *in vitro* and *in vivo* models.

Nanomaterial exposure in pregnant patients is a relatively new field of study. Depending on the properties of specific nanoparticles and the route of exposure, they can exert effects on both the pregnant mother and the fetus [32,35,36]. For instance, respiratory titanium dioxide exposure may cause pulmonary inflammation in pregnant rats, and increase the susceptibility of their pups to allergies [33,37]. Exposure through subcutaneous injection of titanium dioxide may result in accumulation in the fetal brains of mice and can alter normal gene expression causing oxidative stress [33,36,38]. These are some of the many examples suggesting that biocompatibility of certain "inert" nanoparticles can change during pregnancy [37]. Though many studies of nanoparticle toxicity during pregnancy are ongoing, new nanomaterial fabrication and exposure risks are arising faster than these toxicities are being studied [32].

Exposure risks may be particularly important to study when considering nanomaterials that have pharmaceutical applications. Many ongoing projects exist for the development of therapeutic and diagnostic applications. Various routes of nanomaterials

13

administration, including ingestion, injection, inhalation, or transdermal administration are being developed [32]. These materials may have a number of benefits over traditional therapies and diagnostic modalities, including selective tissue administration and improved pharmacokinetic profiles. A number of nanomaterials including biodegradable polymers, albumin nanoparticles, liposomes and micelles are being developed for biomedical applications [39]. Biodegradable polymeric nanoparticles are advantageous because when metabolized they may form secondary compounds that can be further metabolized and easily cleared. Although in some cases the metabolites could be cytotoxic [32]. An example of this is poly(lactide-*co*-glycolide), a polymer that can be formulated into nanoparticles and act as a matrix, housing drug that can be released in a controlled fashion. Several applications of this biocompatible polymer have already been introduced in clinical studies and have even been FDA approved [39]. This polymeric matrix is hydrolyzed to lactic acid and glycolic acid, two compounds that can be further metabolized by the body [39].

An advantage of nanoparticles for therapeutic delivery of drugs is that they can be taken up by endocytosis mechanisms that are otherwise not available to the free drug. Additionally, nanoparticles can be functionalized with surface targeting ligands. These ligands may be small molecules or peptides that interact with tissue specific receptors and allow for selective delivery to tissues requiring the drug [40]. A nanoparticle delivery system could theoretically be used during pregnancy to increase delivery to the fetus by targeting a trophoblast specific receptor.

Hypothesis

The hypothesis driving this project is that digoxin-loaded nanoparticles may be used to selectively target the placenta and increase fetal delivery of digoxin. This project is designed to investigate this hypothesis by addressing the two underlying issues with current fetal digoxin administration.

The first issue that is addressed with this project is whether or not digoxin could theoretically be delivered across the placental trophoblast without efflux by P-gp. We hypothesize that polymeric nanoparticles can be taken up by cells by endocytosis, essentially skipping the transmembrane permeation of free digoxin. P-gp causes efflux of digoxin by either uptake directly from the membrane, or by uptake of free drug from the cytosol. If digoxin-loaded nanoparticles can be taken up by endocytosis, digoxin will not reside in the membrane and thus may be shielded from P-gp efflux.

The second issue that is addressed by this project is whether digoxin delivery could be targeted to the placenta to reduce systemic delivery to the mother. We hypothesize that targeting digoxin-loaded nanoparticles towards folic acid receptors on the placental surface can reduce the maternal plasma concentration of digoxin. Folic acid receptors are present in some tissues, but with very low expression. They are, however, a particularly abundant receptor in the placenta. The reason for the high expression of folate receptors on the placenta is that both the placenta and the fetus require folic acid to develop correctly. It is well known that folic acid supplementation before and during the early phases of pregnancy is necessary for reducing the occurrence of neural tube defects (e.g. spina bifida). Folic acid has been shown to be important in placental development as well [41]. Therefore, nanoparticles with folic acid on the surface should accumulate at this site. In addition, folate receptor-mediated endocytosis is a well known phenomenon of folate receptor-expressing tissues, and may be exhibited by trophoblast cells, further increasing delivery of nanoparticles to the fetus.

15
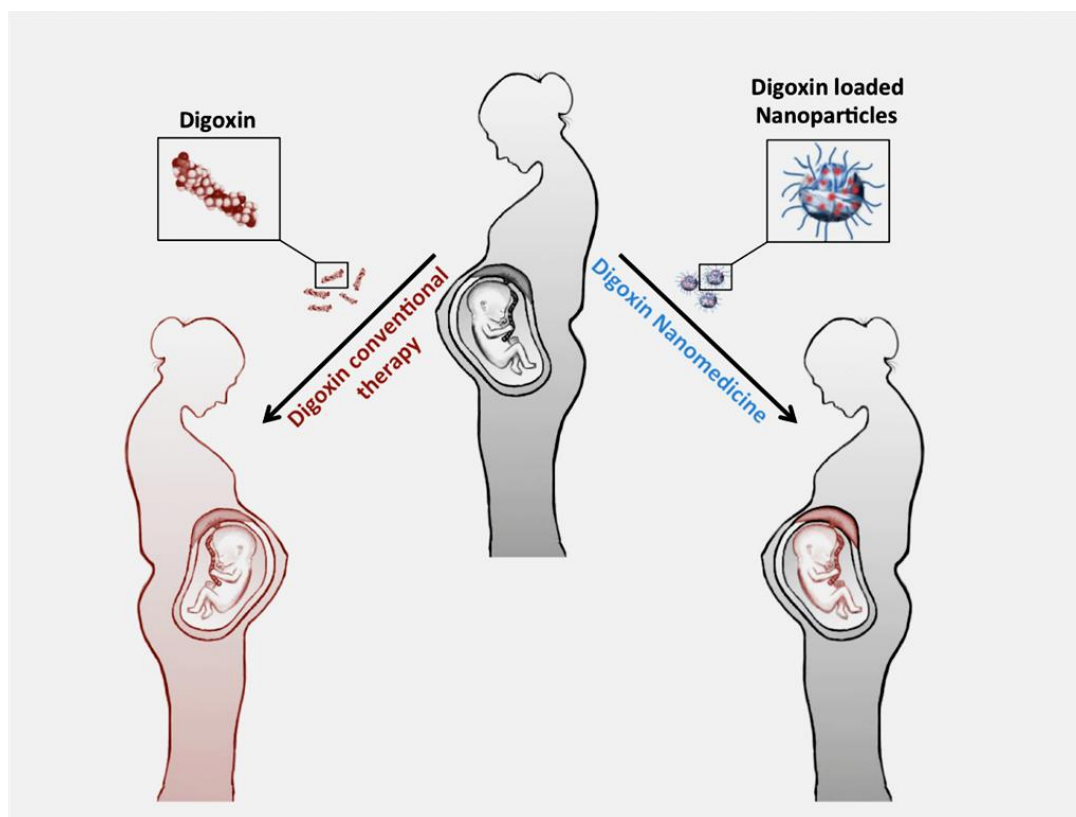
Figure 1.5. Targeted drug delivery in pregnancy.

Nanoparticles for targeted fetal delivery hold the promise of improved fetal delivery of pharmaceuticals, potentially reducing maternal side effects [42].

Though at an early stage, we hope this project will provide a novel, clinically relevant approach for the treatment of fetal arrhythmia. By selectively delivering digoxin

to the fetus, this treatment strategy should be able to reduce maternal toxicity and improve both maternal and fetal outcomes. Fetal arrhythmias and fetal congestive heart failure are relatively common diseases and can be lethal if not treated in a timely or effective manner. We also believe that this project will increase our understanding of the behavior of nanoparticle drug formulations, as well as shed light into the interaction of nanoparticles with the placenta and the potential utility of nanoparticles in the delivery of other drugs to the fetus.

Chapter 2: Transport of digoxin-loaded polymeric nanoparticles across BeWo cells, an *in vitro* model of human placental trophoblast

INTRODUCTION

As stated in the introduction, fetal cardiac arrhythmias occur in 1% of pregnancies and can result in fetal heart failure [1,2,43]. Arrhythmias also represent a leading cause of fetal hydrops, which has an incidence of one in 2500 pregnancies [2,7] and high mortality [7,8]. Digoxin is the drug of choice for treating fetal tachyarrhythmias and fetal congestive heart failure [44]. Maternally administered digoxin has been shown to be effective in terms of conversion of supraventricular fetal tachycardias to normal sinus rhythm [2]. Still, fetal death occurs in about 10% of fetal tachyarrhythmia cases, and more in hydropic fetuses. Transplacental digoxin treatment is 71% effective in cases involving nonhydropic fetuses and 10% effective in hydropic fetuses [9]. Transplacental transfer of digoxin to the fetus is limited because digoxin is a substrate for the efflux transporter P-glycoprotein (P-gp), which is highly expressed in human placenta [45], and is also expressed in BeWo cells [46]. Prenatal digoxin therapy can lead to undesirable side effects for the mother, because the majority of the dose remains in the maternal circulation due to P-gp efflux [18]. There is a great need to improve the delivery of digoxin to the fetus and simultaneously minimize maternal drug exposure.

Previous work has demonstrated that polymeric nanoparticles with diameters ranging around 100 nm can cross the placental barrier [47]. The hypothesis driving this project is that an innovative, nanoparticle-based approach could improve the transplacental delivery of digoxin to the fetus. Such an approach may improve fetal digoxin therapy by means of reduced interactions of nanoencapsulated digoxin with P-gp,

resulting in more efficient transplacental transfer of digoxin to the fetus. This strategy could have major implications in future therapy for fetal arrhythmias. Targeted delivery of digoxin to the fetus may lower the risk of maternal complications during pregnancy as well. Thus, the studies described herein are intended to fill a critical void in fetal cardiovascular therapy during pregnancy and improve cardioversion to normal sinus rhythm. Biocompatible and biodegradable polymeric nanoparticles containing digoxin have been prepared and characterized in terms of particle size, encapsulation efficiency, and drug release. These nanoparticles are advantageous because they are composed of a copolymer of polyethylene glycol (PEG) and poly(lactic-*co*-glycolic acid) (PLGA), the structure of which is shown in **Figure 2.1**.
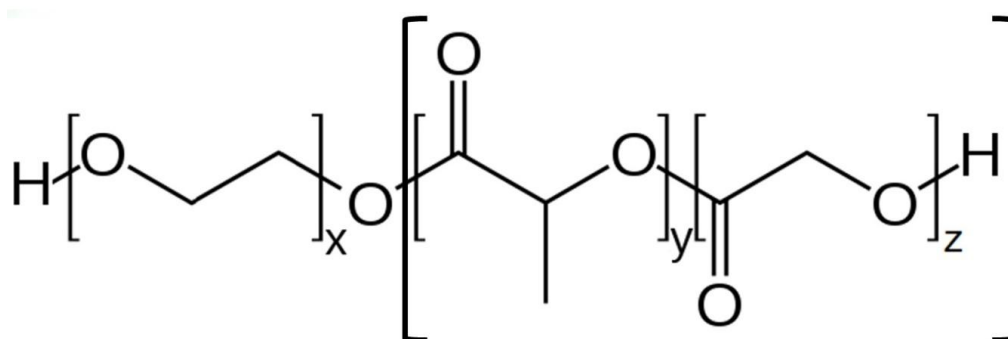
Figure 2.1. Structure of PEG-PLGA.

PEG is composed of X units of ethylene glycol, while PLGA is composed of Y units of lactic acid and Z units of glycolic acid [48].

PLGA is biodegradable material already present in many formulations approved by the FDA and the European Medicine Agency [39]. In addition, PLGA is known for its excellent controlled release characteristics [49]. The transport of digoxin as free drug or encapsulated in nanoparticles was compared using the BeWo b30 cell line, an *in vitro* model of human placental trophoblast cells separating the maternal and fetal circulations [26]. Finally, the effect of nanoencapsulation on the interaction of digoxin with P-gp was investigated by means of transport studies in the presence of verapamil, a P-gp inhibitor [50].

MATERIALS AND METHODS

Preparation of nanoparticles

Nanoparticles were prepared by a modified solvent displacement method, as described elsewhere [51]. Briefly, solutions of PEGylated poly (lactic-*co*-glycolic acid) polymer (Resomer® RGPd50105 and RGPd5055, Boehringer Ingelheim, Ingelheim am Rhein, Germany) were prepared at concentrations of 3 mg/mL in tetrahydrofuran (THF, Acros Organics, Geel, Belgium), along with digoxin (MP Biomedicals, LLC, Santa Ana, CA) at 5 and 10% theoretical drug loading, and allowed to mix overnight. The solutions (1 mL) were nanoprecipitated in 5 mL purified water by injection through a 22-gauge needle (0.7mm x 40mm, PrecisionGlide Needle®, BD, Franklin Lakes, NJ) with a variable-speed peristaltic pump (Traceable® Calibration Control Company, Friendswood, TX) at a rate of 6.0 mL/min. During the injection, the suspension was stirred at 500 rpm on a magnetic stir plate. Following precipitation, suspensions were allowed to stir at 850

rpm until THF had completely evaporated (at least 8 hours, confirmed by HPLC). Volumes were then completed to 5 mL using purified water [52].

High performance liquid chromatography

Digoxin concentrations were determined using reversed-phase high performance liquid chromatography (HPLC), similar to the method of Hu et al. (Hu et al. 2010). Flow was established using a binary pump (1500-series HPLC pump, Waters, Milford, Massachusetts) at 1 ml/min in isocratic conditions of 30:70 (v/v) acetonitrile to purified water, with a C18 Symmetry® column (5μm, 4.6 mm x 150 mm, Waters, Milford, MA), at room temperature. Detection was at a wavelength of 230 nm using a Waters 2998 photodiode array detector (Milford, MA), and the method was validated.

Nanoparticle characterization

Suspensions of the nanoparticles were characterized using a high performance particle sizer (HPPS, Malvern Instruments, Malvern, UK) to determine particle size and polydispersity index (PDI). Zeta potential was determined using a Zetasizer 2000 (Malvern Instruments, Malvern, UK).

Thermal properties of nanoparticles were determined with a Q200 differential scanning calorimeter (TA Instruments, New Castle, DE). Differential scanning calorimetry allows one to determine the glass transition temperature of the polymer, which is the temperature at which a polymer changes from a hard, glassy state to a soft, rubbery state. Nanoparticle suspensions were lyophilized using a FreeZone 2.5L benchtop freeze dry system (Labconco, Kansas City, MO). Following lyophilization, nanoparticle samples were collected and samples (1-8 mg) were placed in sealed aluminum hermetic sample pans, and scanned from 0°C to 300°C at a rate of 10°C/min.

Encapsulation efficiency was determined by HPLC. Non-encapsulated digoxin was separated from the nanoparticles by placing 500 μL of the suspensions into Amicon® Ultra-0.5 centrifugal filters (100,000 MWCO, Tullagreen, Ireland) spun at 10,000 × g for 15 minutes using an Eppendorf ® 5430 centrifuge (Hamburg, Germany). Nanoparticles in the aqueous nanosuspension do not pass through the filters. The filtrate, which contains the unencapsulated drug in the nanosuspension, was analyzed by HPLC, and encapsulation efficiency was calculated as described previously [53], with correction for any nonspecific binding of digoxin to the filter membranes.

Drug release

Release of digoxin from the nanoparticles was studied in phosphate buffered saline (PBS) at 37°C as described previously [54]. Briefly, 1.5 mL of aqueous nanosuspension (nanoparticles prepared at 10% drug loading) were added to 13.5 mL of 1.11X PBS (so that the final mixture was 1X PBS) at time zero. The mixture was rotated at 75 rpm (Junior Orbit Shaker, Lab-Line, Melrose, Illinois) in a mini-incubator (Boekel, Feastervillle, PA). Samples were taken at the specified time points and placed in centrifugal filters, which were spun at 4000 rpm for 10 minutes at 25°C in an Eppendorf ® 5810R centrifuge. The filtrates of samples taken in triplicate were analyzed by HPLC to quantify the amount of drug released from the nanoparticles over time.

Cell Culture

BeWo cells retain trophoblastic transport characteristics and phenotype, including the expression of P-glycoprotein [55]. BeWo cells (b30 clone, obtained from Lisbeth Knudsen, University of Copenhagen, Denmark) were cultured in DMEM/F-12 media (Dulbecco's Modified Eagle's Medium/Ham's F-12 50/50 mixture, Mediatech,

Manassas, VA) containing 10% fetal bovine serum (Atlanta Biologicals, Lawrenceville, GA), antibiotic/antimycotic (containing 10,000 units/mL penicillin, 10,000 μg/mL streptomycin, and 25 μg/mL amphotericin B, Gibco®, Life Technologies, Carlsbad, CA), 100X MEM non-essential amino acid solution (Sigma, St. Louis, MO), and 200 mM L-glutamine (Cellgro, Corning, NY). Cells were revived from an aliquot stored in liquid nitrogen (passage number 29) and grown in a 95% humidified incubator with 5% CO_2 at 37° C. At confluence (80-90%), cells were seeded at a density of 224,000 cells/mL in polycarbonate Transwell® inserts (pore size 3 μm, growth area 1.12 cm^2, apical volume 0.5 mL, basolateral volume 1.5 mL, Corning, NY) coated with human placental collagen type IV (Sigma, St. Louis, MO) in preparation for transport studies as described previously [56]. Cell culture media was changed daily. A continuous trophoblast layer is important in the protective function of the placenta [57], and therefore, transepithelial electrical resistance (TEER) measurements were used to measure the integrity of cell monolayers [53]. TEER values were measured using an EndOhm® voltohmmeter (World Precision Instruments, Sarasota, FL), at 25° C starting on day 4 post-seeding to ensure monolayer formation. TEER values between 30 and 60 Ω·cm2 (corrected for resistance of collagen coated Transwell inserts without cells) were considered acceptable for performing transport studies (which were performed on day 6 post-seeding) [58]. Each set of cells grown on the Transwell inserts had similar TEER values.

Cytotoxicity

The cytotoxicity of blank PEGylated PLGA nanoparticles in BeWo cells was measured at 4, 24, and 48 hours after exposure to ensure nanoparticle toxicity would not contribute to alterations in trophoblast monolayer integrity. This was measured by a well established colorimetric assay based on a water soluble tetrazolium salt (4-[3-(4-iodophenyl)-2-(4-nitrophenyl)-2H-5-tetrazolio]-1,3-benzene   disulfonate,   or   WST-1)

(Ishiyama et al. 1996). Cells were seeded in 96 well plates at a density of 4.0125 x 10^5 cells/well (well surface area = 0.321 cm^2) and allowed to grow for 48 hours. Blank nanoparticle treatments were then added to appropriate wells and allowed to incubate for either 4, 24, or 48 hours before addition of 110 µL of X mM WST-1. Cells were then allowed to incubate for an additional 2 hours at 37° C, and absorbance of the WST-1 metabolite was measured using a plate reader at 420-480 nm. Cells were treated with blank media as a negative control and 0.1% Triton X-100 as a positive control [59].

Transport studies

Transport studies were conducted using BeWo b30 cells following the protocol of Cartwright et al. with slight modifications [47]. After ensuring the formation of monolayers in each Transwell, 0.5 mL of cell culture media containing each digoxin formulation to be compared was placed in the apical side of the respective Transwell inserts. The inserts were maintained at 37°C in cell culture conditions (95% relative humidity, 5% CO_2) and stirred at 50 rpm with an orbital shaker. Samples (200 µL) were collected at the specified time points from the basolateral chamber and analyzed by HPLC. Cell culture media (200 µL) was replaced immediately following each sample from the basolateral chamber to maintain volume. Mass transfer and the apparent permeability (Pe, or the permeability of the drug across the cell layer corrected for the permeability across the blank collagen coated Transwell insert) of digoxin was calculated and corrected for mass removed during sampling as described previously [47].

Statistical analysis

Averages and standard deviations were calculated for each experimental group in an experiment, including cytotoxicity and permeability. Data were analyzed using the Student's t-test between designated groups, with a p-value less than 0.05 considered a significant difference.

RESULTS

High performance liquid chromatography

In reversed phase HPLC, a mobile phase is passed across a stationary phase (silica) coated with hydrophobic chains (saturated 18 carbon chains), as shown in **Figure 2.2**. Hydrophobic characteristics of analytes cause variable retention in the column. A high performance liquid chromatography method was developed and validated for the detection of digoxin at a wavelength of 230 nm (see Figure 2.3, Table 2.1). The method was checked for accuracy and precision, and the limit of detection was determined to be 24 ng/mL. Short term stability of samples was also assessed. The method was validated using both 50:50 F12:DMEM cell culture media (applicable to the transport studies) and purified water (applicable to the determination of encapsulation efficiency).
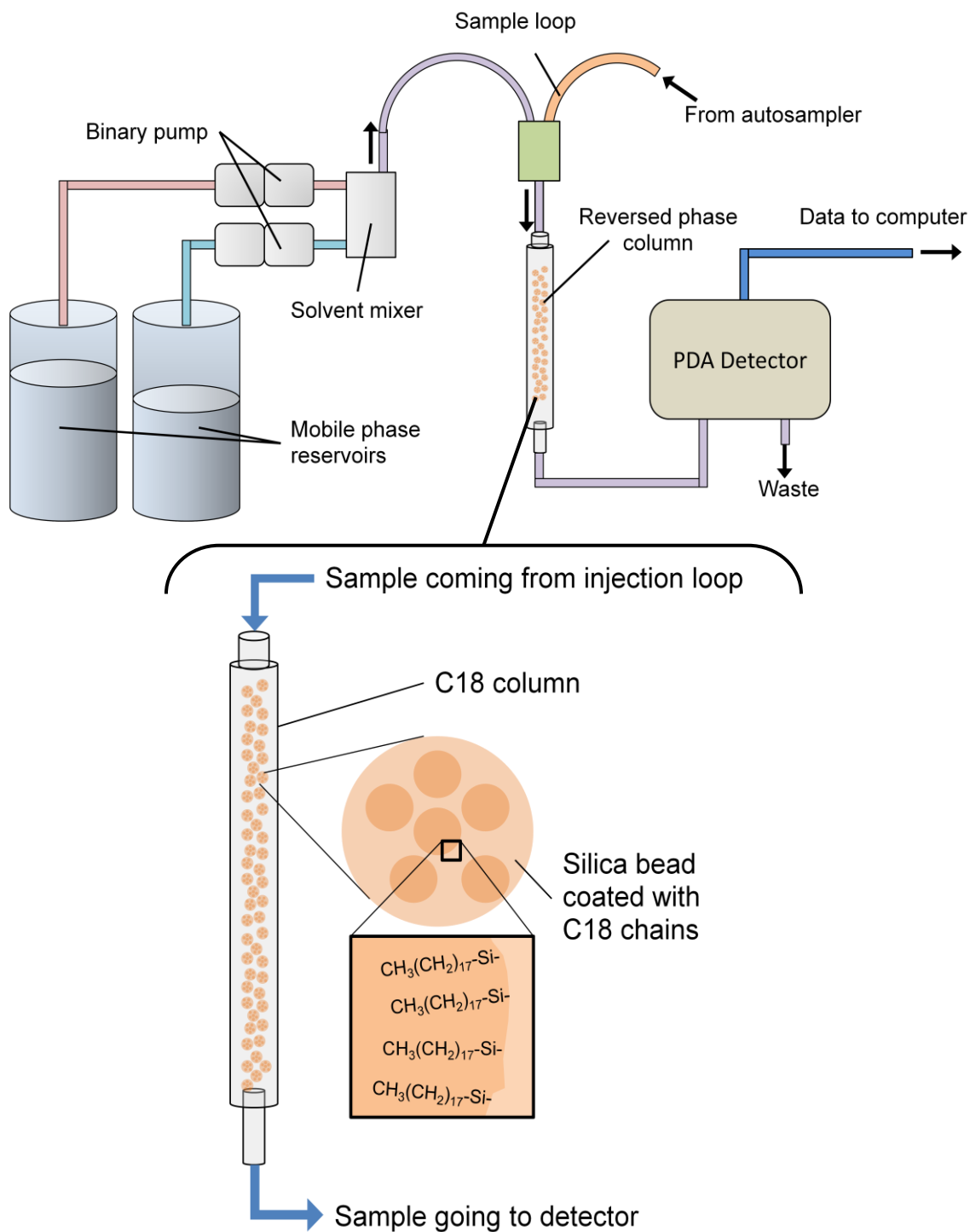
Figure 2.2. Reversed phase HPLC with C-18 column and photodiode array detector.

Two solvent reservoirs typically hold an aqueous and an organic solvent that are mixed.
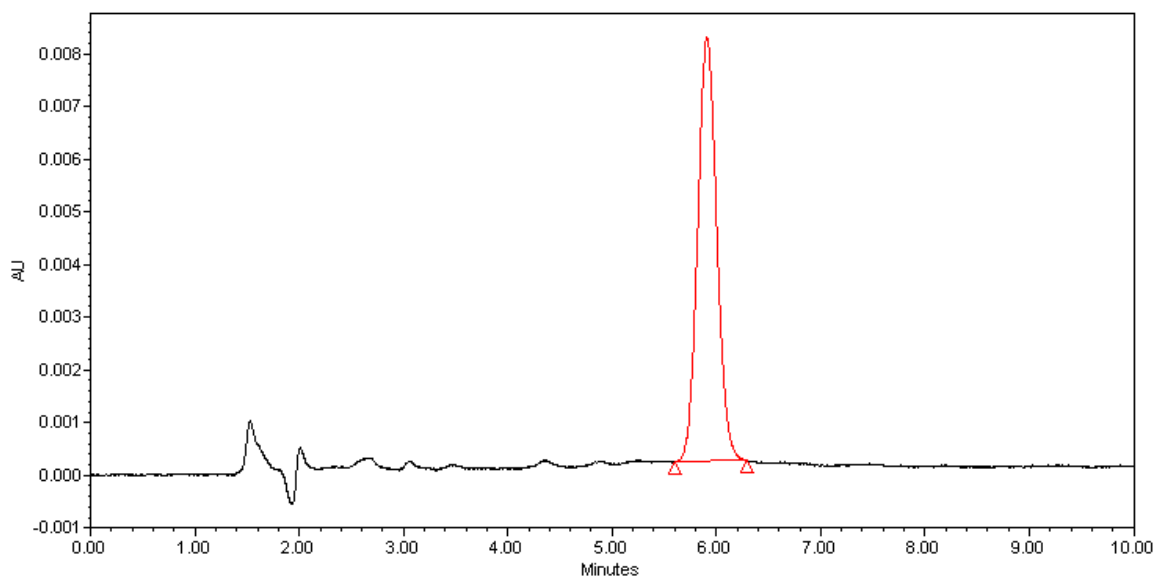
Figure 2.3. Chromatogram showing selectivity of method for digoxin detection.

Detection of digoxin in cell culture media was by PDA detector at 230 nm. Retention time was approximately 6 minutes.

Table 2.1. Short-term (3 day) sample stability at room temperature and validation of the HPLC method for digoxin (% CV = coefficient of variation).

Nominal Concentration (µg/mL)		0.5	5	10	50
Day 1	**Mean**	0.486	5.087	10.079	49.975
	% CV	1.4	0.8	0.1	1
	% Accuracy	97.3	101.7	100.8	100
Day 2	**Mean**	0.475	5.21	10.257	51.243
	% CV	0.8	0.1	0	0.1
	% Accuracy	95.1	104.2	102.6	102.5
Day 3	**Mean**	0.493	5.128	10.085	49.887
	% CV	0.2	0.5	0.2	0.9
	% Accuracy	98.7	102.6	100.9	99.8

Table 2.2. Physicochemical characterization and encapsulation efficiency of PEG-PLGA nanoparticles loaded with digoxin.

Formulation: Polymer (drug loading)	Z-average particle size (nm)	Polydispersity index (PDI)	Zeta potential (mV)	Encapsulation efficiency (%)
RGPd50105 (5%)	64 ± 0.4	0.19 ± 0.00	-14 ± 14	>97.4
RGPd50105 (10%)	84 ± 0.4	0.25 ± 0.02	-9 ± 11	98.4 ± 0.2
RGPD5055 (5%)	123 ± 0.7	0.22 ± 0.01	-48 ± 2	>97.4
RGPd5055 (10%)	124 ± 1	0.22 ± 0.01	-47 ± 3	94.9 ± 0.7

a. Polymer is 10% PEG and 90% PLGA by weight.

b. Polymer is 5% PEG and 95% PLGA by weight.

Table 2.3. Physicochemical characterization and encapsulation efficiency of digoxin-loaded RGPd50105 nanoparticles with various levels of theoretical drug loading.

Theoretical drug loading (%)	Z-average particle size (nm)	Polydispersity index (PDI)	Zeta potential (mV)	Encapsulation efficiency (%)
1	155.9 ± 3.5	0.14 ± 0.03	-46.9 ± 4.6	>86.6
3	137.4 ± 7.2	0.15 ± 0.01	-41.3 ± 3.8	77.7 ± 1.5
5	192.3 ± 13.3	0.05 ± 0.01	-44.3 ± 2.6	>97.4
10	125.6 ± 3.9	0.19 ± 0.01	-38.8 ± 5.2	98.4 ± 0.2
15	149.4 ± 5.8	0.14 ± 0.04	-45.6 ± 1.4	95.1 ± 0.1

Nanoparticle characterization

Digoxin-loaded polymeric nanoparticles were prepared by a modified solvent displacement method. Two different polymers and various percentages of theoretical drug loading were screened (see **Tables 2.2** and **2.3**). **Table 2.2** shows that greater than 90% encapsulation efficiency was observed for both polymers at drug loading values of 5% and 10%. Increased PEG content of the polymer resulted in less negative zeta potential values, and the polydispersity index values were all less than or equal to 0.25, indicating monodisperse nanosuspensions. Differential scanning calorimetry studies confirmed encapsulation of the drug within the nanoparticles. The decrease in glass transition temperature (Tg) with increased drug loading shown in **Table 2.4** suggests a solid dispersion of digoxin in the polymer matrix [60].

Release Study

The release study for digoxin loaded nanoparticles was conducted in PBS at 37°C under sink conditions, using centrifugal filters (MWCO 100,000) to separate nanoparticles from released digoxin. **Figure 2.4** demonstrates sustained release over the 48-hour study period, with no initial burst release. The classical Higuchi model for drug release correlates the percentage of drug released to the square root of time, as follows: $M_t/M_\infty = K(t)^{1/2}$, where M_t is the mass of drug released at time t, M_∞ is the total cumulative mass of drug released at infinite time, and the constant K is dependent on experimental variables [61,62]. The data from the release study were fit to the Higuchi model for drug release. The inset to **Figure 2.4** shows that for this nanoparticle formulation, $K=0.074$ ($R^2 = 0.998$). The value of the intercept of the fitted line (4.2%) is similar to the amount of unencapsulated drug determined experimentally (100% – the encapsulation efficiency), providing further evidence of inconsequential burst release.

Table 2.4. Glass transition temperatures (T_g) of digoxin-loaded nanoparticles.

Glass transition temperatures of blank nanoparticles (no drug loading) and digoxin-loaded PEG-PLGA (RGPd50105) nanoparticles were determined by differential scanning calorimetry.

Sample	T_g (°C)
Blank nanoparticles	33.3
Digoxin-loaded nanoparticles (5% drug loading)	32.3
Digoxin-loaded nanoparticles (10% drug loading)	28.6
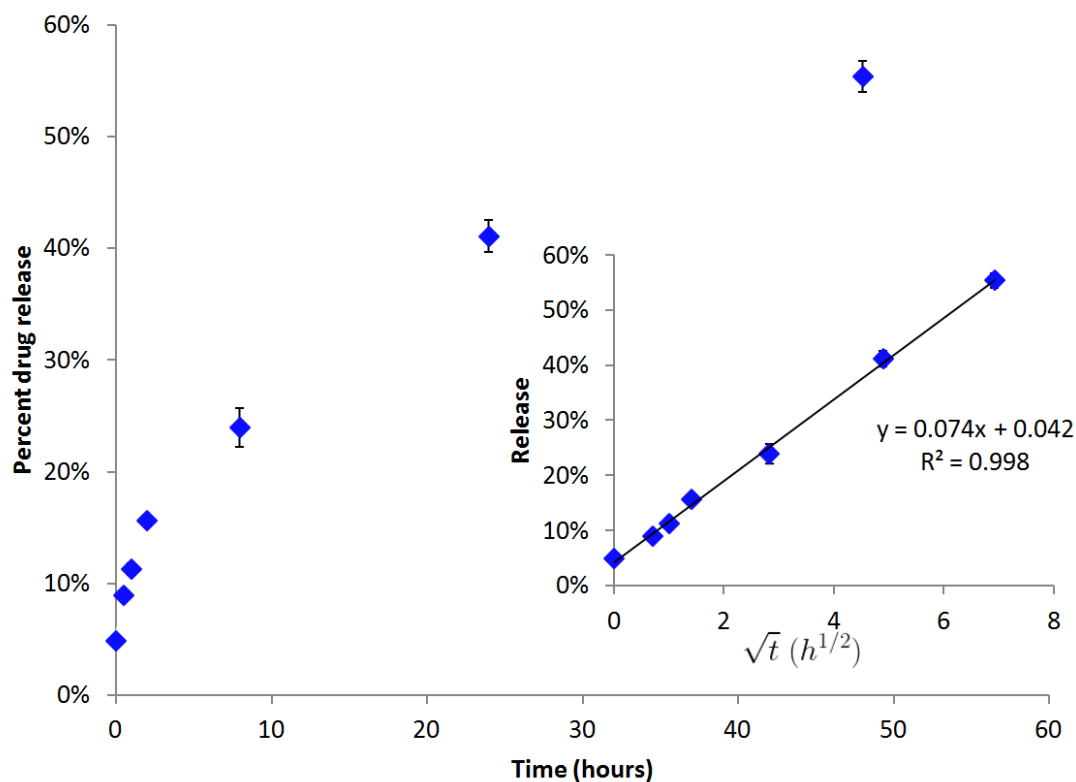
Figure 2.4. *In vitro* drug release of digoxin from PEG-PLGA nanoparticles.

Drug release was measured (RGPd50105, 10% drug loading) over 48 hours under sink conditions at 37°C in phosphate buffered saline. The inset shows the fit of the data to the Higuchi equation (see text). Error bars represent the standard deviation (n=3).

Cytotoxicity

Cytotoxicity of blank nanoparticles in BeWo cells was measured using the well established WST-1 colorimetric assay (**Figure 2.5**). 0.1% Triton X-100 was used as a positive control, and blank media was used as a negative control (i.e., 100% cell viability). **Figure 2.6** shows that no significant cytotoxicity was seen at 4, 24, or 48 hours for any of the concentrations of blank nanoparticles tested. This indicates that any

permeability differences in transport studies are not attributed to cytotoxicity effects of nanoparticles on cells.
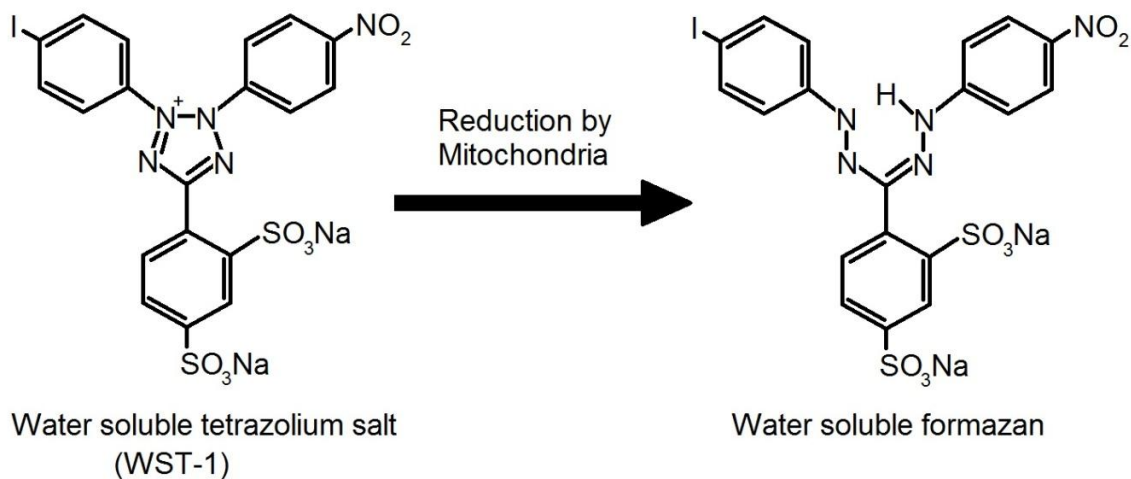
Figure 2.5. Colorimetric WST-1 assay.

Viable cells are able to reduce the water soluble tetrazolium salt to a water soluble formazan.

Transport studies

Transport studies were conducted by dosing treatments to the apical (maternal) side of the BeWo cells on Transwell inserts and measuring the basolateral (fetal side) concentrations of digoxin by HPLC at pre-specified time points. Average TEER values for all groups were between 41.7 and 44.2 $\Omega \cdot cm^2$. Treatments were administered at a dose of 7.2 μg/mL of digoxin for all transport studies. Apparent permeability (*Pe*) at 2 hours (a time point at which the mass flux was linear) was calculated from the concentration of drug in the basolateral chamber [47]. **Figure 2.7** shows that encapsulation

of digoxin in nanoparticles resulted in an increase in the apparent permeability of the drug in the apical (maternal) to basolateral (fetal) direction by 2.5-fold (p<0.05). The transport studies were repeated in the presence of 100 µM verapamil, a P-gp inhibitor [50]. A significant difference was also seen between permeability values of free digoxin and free digoxin in the presence of inhibitor.
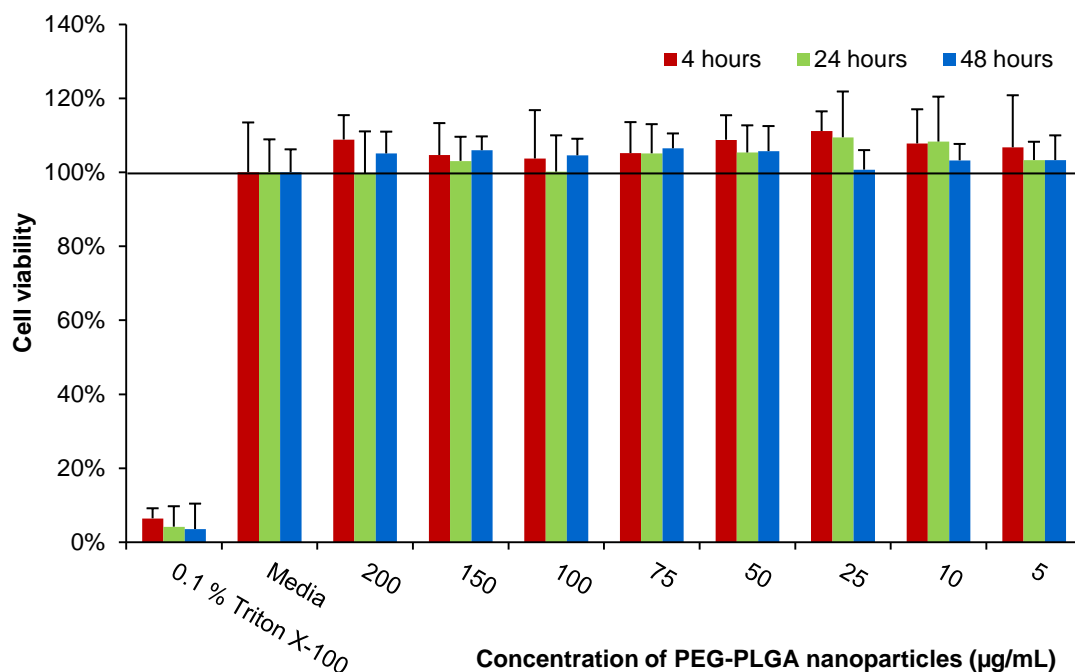
Figure 2.6. *In vitro* cytotoxicity of PEG-PLGA nanoparticles at various concentrations.

Cell viability at 4, 24, and 48 hours in the presence of blank PEG-PLGA nanoparticles was measured using the WST-1 assay. Cell viability is presented as a percent of the viability of the cells cultured in blank media at the respective time point.
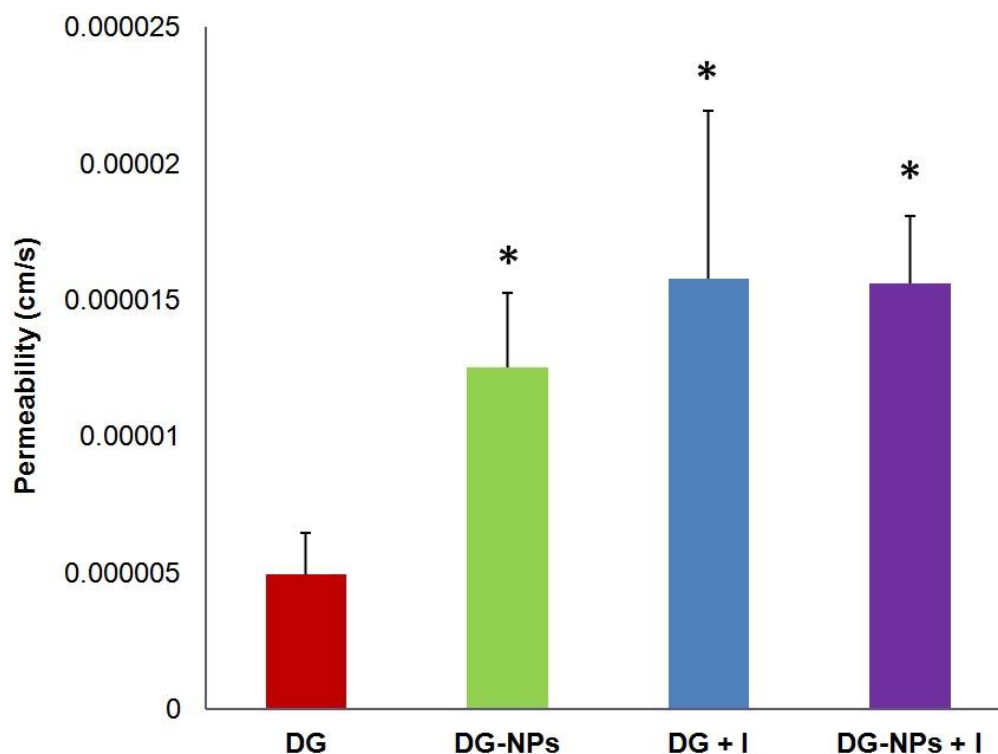
Figure 2.7. Permeability of digoxin-loaded nanoparticles in the presence and absence of verapamil.

Apparent permeability (Pe) for the transport of free digoxin (red bar) and digoxin-loaded PEG-PLGA nanoparticles (RGPd50105, 10% drug loading, green bar) across BeWo cell monolayers in the apical (maternal) to basolateral (fetal) direction at the 2-hour time point. The transport studies were carried out at 37°C under cell culture conditions, with stirring. Pe was also determined for both formulations in the presence of 100 μM verapamil, a P-gp inhibitor. Asterisks indicate significant differences from the permeability of free digoxin ($p < 0.05$). There were no significant differences between the Pe values of the digoxin-loaded nanoparticles, free digoxin in the presence of the P-gp inhibitor ("I") verapamil (blue bar), or digoxin-loaded nanoparticles in the presence of verapamil (purple bar). Error bars indicate standard deviation (n=3).
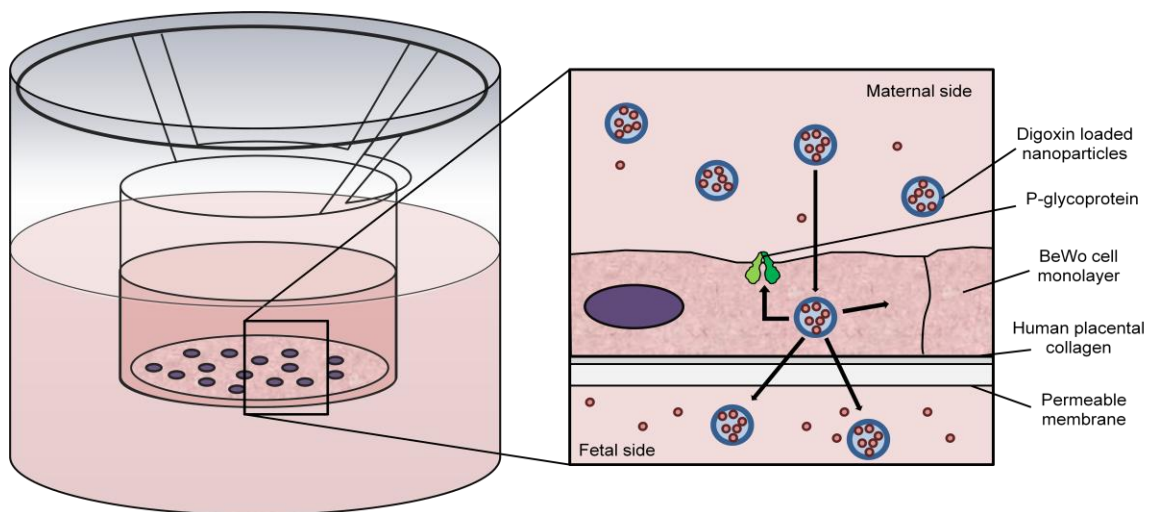
Figure 2.8. Tranwell insert.

Transport studies are conducted on Transwell inserts coated with human placental collagen. BeWo cells are seeded on the membrane, and drug permeability is calculated by measuring digoxin concentrations in the basolateral media (fetal side).

DISCUSSION

Fetal cardiac arrhythmia is not easily managed, and treatment often causes severe and unintentional maternal effects. Although digoxin can be used to treat fetal arrhythmias, the placenta as an anatomical barrier between the mother and the fetus limits the maternal-to-fetal transfer of this particular drug, such that a substantial fraction of the dose remains in the maternal circulation. Efflux mechanisms in the placenta (such as P-

gp) restrict the passage of digoxin to the fetal circulation. This study was conducted to show that polymeric nanoparticles may present an alternative treatment strategy to deliver digoxin and improve therapy in fetal cardiac arrhythmia. It is widely known that PLGA and PEG are biocompatible polymers and have been previously approved by the FDA for delivery applications [39]. PEGylation improves nanoparticle pharmacokinetics by reducing opsonization [47,63]. Our experiments have also confirmed that PLGA-PEG nanoparticles are not cytotoxic to trophoblast cells, and are therefore an ideal drug delivery platform.

It has previously been shown that polymeric particles approximately 100 nm in diameter can cross the placenta [47,63]. In this work, digoxin-loaded nanoparticles were synthesized by a modified solvent displacement method, which resulted in high encapsulation efficiency, narrow polydispersity, and appropriate particle size to promote transplacental drug delivery.

One advantage of nanoparticles for drug delivery is controlled release of the drug from the nanocarriers [64]. Sustained release of the drug over time can reduce the required dosing frequency, which improves patient convenience. We observed a sustained release of the digoxin from the polymeric nanoparticles (**Figure 2.4**). The lack of substantial burst release is also advantageous, as the drug release kinetics may be used to predict the pharmacokinetics of the drug when delivered as a nanoformulation.

Nanoparticles may also address the challenge of reduced transplacental transfer of digoxin due to P-gp-mediated efflux of the drug within trophoblast cells, which represent the rate-limiting layer of the maternal-fetal interface. BeWo cells express functional P-gp, and therefore would be an appropriate *in vitro* placental trophoblast model [46]. **Figure 2.7** shows that the encapsulation of digoxin in PEG-PLGA nanoparticles resulted in a 2.5-fold increase in the apparent permeability (P_e) of digoxin across BeWo cells in the maternal-to-fetal direction. We hypothesized that the nanoparticles may result in increased transfer of digoxin across trophoblast cells by reducing the interaction of the

drug from the efflux transporter P-glycoprotein. We further predict that nanoparticles themselves cross the BeWo cell layer, as was shown previously using fluorescent PLGA nanoparticles [53]. **Figure 2.10** illustrates the concept of nanoparticle encapsulation effectively shielding the drug from being recognized and effluxed by P-gp. **Figure 2.9** depicts the efflux of digoxin, which reduces the accumulation and transport of digoxin into and across the trophoblast cell layer. **Figure 2.10 (A)** represents the increased permeability of digoxin in the presence of a P-gp inhibitor. **Figure 2.10 (B)** portrays the shielding of digoxin from interaction with P-gp when the drug is encapsulated in the nanoparticles. Each nanoparticle carries multiple drug molecules into and across the trophoblast cell barrier. In line with this hypothesis, we observed the significantly increased permeability upon nanoencapsulation of digoxin was similar to the magnitude of increased permeability obtained when inhibiting P-gp by the co-administration of 100 μM verapamil. As illustrated in **Figure 2.10 (B)**, the fraction of drug molecules that has already been released from the nanoparticles may still be susceptible to P-gp-mediated efflux. (For example, **Figure 2.4** shows that after 2 hours—the time point at which Pe was determined in the transport studies—approximately 16% of the drug has been released). This is represented experimentally as the small (but not statistically significant) difference in the apparent permeability of digoxin when encapsulated in nanoparticles administered in the presence of verapamil (the blue bar in **Figure 2.7**) minus the permeability of the nanoencapsulated drug in the absence of verapamil (the green bar in **Figure 2.7**). It should also be noted that differences in permeability may also be due to differences in transport mechanisms for nanoparticles, such as endocytosis [65]. Examination of these mechanisms would include selective inhibitors of different modes of endocytosis (e.g. nystatin and chlorpromazine to inhibit caveolae and clathrin mediated endocytosis, respectively) [66].
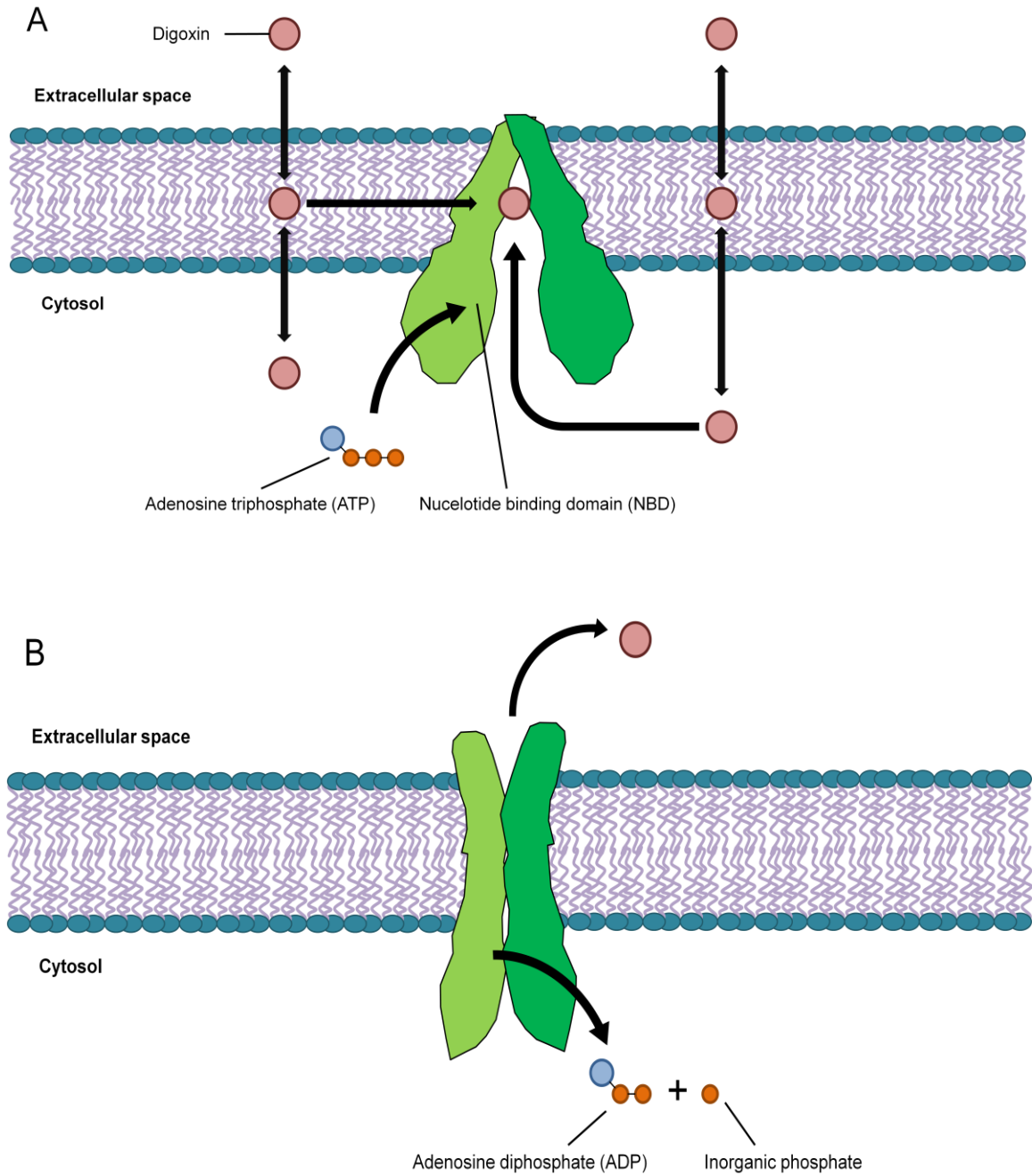
Figure 2.9. Function of P-gp.

(A) P-gp (green) can bind drugs such as digoxin either through the membrane or entering the port on the cytosolic portion of the membrane, and can bind to ATP at the nucleotide binding domain. (B) ATP is hydrolyzed to ADP, giving P-gp the energy required to extrude digoxin.
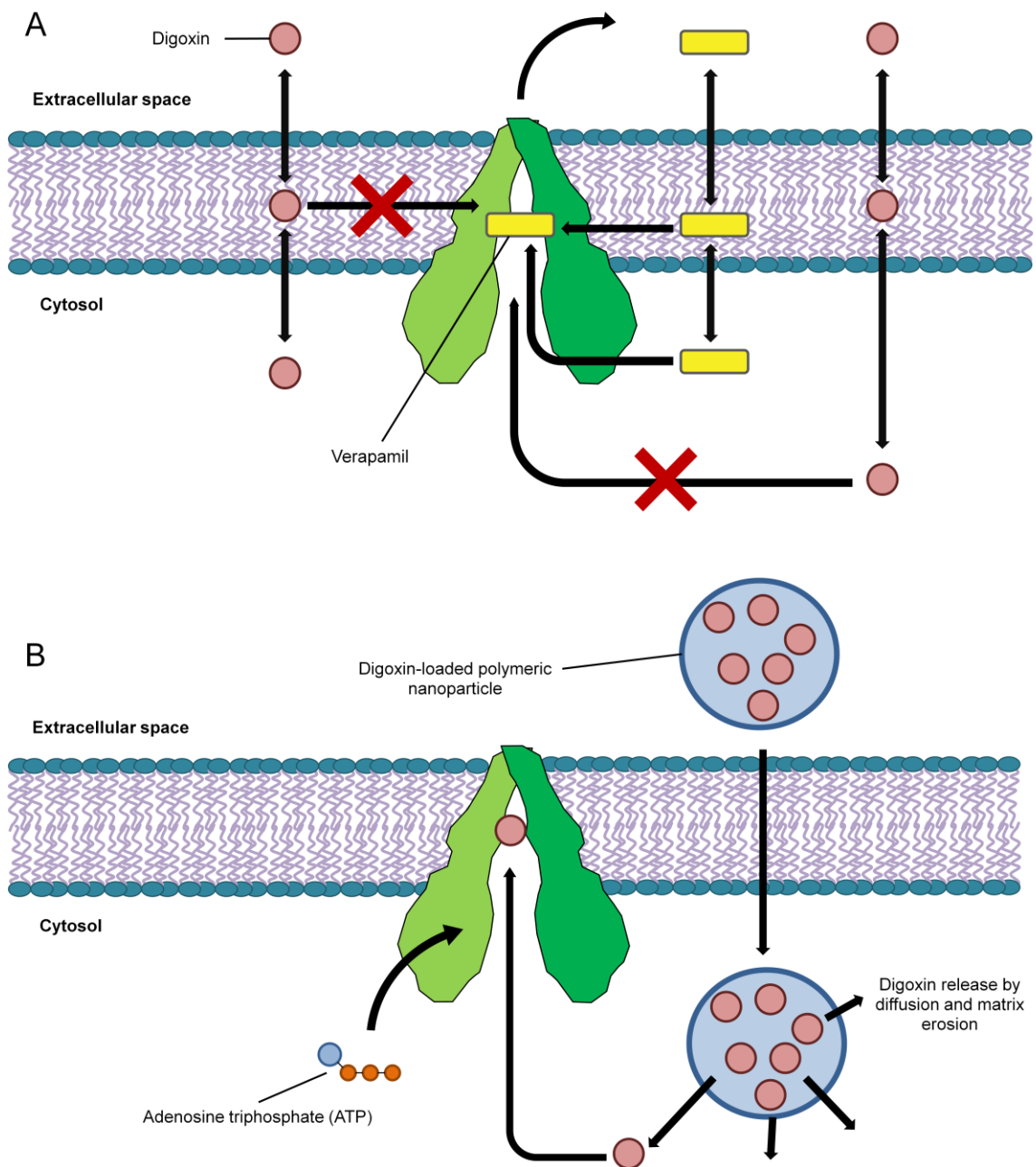
Figure 2.10. Overcoming P-gp with verapamil or nanoparticles

(A) Verapamil, a P-gp inhibitor, is capable of blocking P-gp substrates from entering the drug binding pocket, inhibiting efflux. (B) Polymeric nanoparticles are taken up by endocytosis and can effectively shield digoxin from efflux by preventing entry of digoxin into P-gp via the cell membrane.

CONCLUSION

In conclusion, this study provides a novel approach to the treatment of fetal cardiac arrhythmia. This is a life threatening condition for the fetus, and although treatment with digoxin represents standard treatment and is often successful, it can cause severe side effects in the mother [18]. We have demonstrated that polymeric (PEGylated PLGA) nanoparticles can be successfully loaded with digoxin with high encapsulation efficiency using a modified solvent displacement method. These nanoparticles exhibit sustained drug release kinetics, and nanoencapsulation can protect digoxin from P-gp-mediated efflux in the placental trophoblast layer, thereby increasing the maternal-to-fetal transfer of the drug, which is desired to optimize fetal drug therapy. Increased delivery of digoxin, to the fetus, will result in lower levels of the drug in the maternal circulation, which should result in reduced risks for the aforementioned maternal side effects. The next step in the development of this strategy is to functionalize nanoparticles with ligands that can further induce targeted uptake of the nanoparticles in the placenta. The use of polymeric nanoparticles encapsulating digoxin to treat fetal cardiac arrhythmia may significantly improve outcomes for both the mother and her fetus.

Chapter 3: Synthesis and characterization of folate-targeted nanoparticles loaded with digoxin

INTRODUCTION

This portion of the project is geared towards the development of materials that will be used to develop targeted digoxin delivery formulations for the fetus. An ideal target for this type of delivery is a cell surface protein specific to the placental tissue that, when activated with a particular ligand, would result in increased endocytosis of nanoparticles. Folate receptors fit these criteria.

There are two major types of folate receptors. Folate receptor α is expressed in tissues such as the epithelium of the lung, some glandular tissue, and the placental trophoblast. Folate receptor β is expressed largely on hematopoietic cells [67]. Though both types of folate receptor are expressed in whole placental tissue, the placental trophoblast in particular expresses only folate receptor α [68]. In fact, folate receptor expression levels are much higher in the placenta than any other tissue, as shown by mRNA measurements [68]. The developing fetus requires folic acid, particularly in the beginning stages of gestation, for neural tube development. In fact, folate deficiency during pregnancy has been linked to low birth weight and spinal cord malformations such as spina bifida. Thus, folate receptor expression in the placenta has a crucial role in prenatal development [69].

When folic acid binds to the receptor, it triggers the cell membrane to invaginate and create an endosome. This property of folate receptor-expressing tissues has already

41

been exploited for drug delivery purposes using folate covalently bound to a small molecule drug with an acid-sensitive linker [67]. Additionally, folate receptor-mediated endocytosis of nanoparticles is a new phenomenon that is being investigated for the purposes of drug delivery, though this is mainly focused on pathologic folate expression in cancerous tissues [70]. Folate receptor-mediated endocytosis of nanoparticles has been shown to be a successful targeting strategy for the delivery of chemotherapeutics. Nanoparticles with folic acid bound on the surface are more rapidly internalized by folate receptor-expressing cells [71].

Our hypothesis is that, due to the high expression of folate receptors in the placenta, folate-targeted drug delivery by polymeric nanoparticles may increase the transplacental transfer of digoxin. In addition to shielding digoxin from P-gp (as shown in non-targeted PEG-PLGA nanoparticles), this would theoretically decrease maternal availability of the drug and increase the delivery of drug to the fetus. To prepare folate-targeted digoxin-loaded nanoparticles, we evaluated two methods of synthesizing Folate-PEG-PLGA by the covalent attachment of amine-PEG-Folate to carboxylic acid-terminated PLGA (**Figure 3.1**), both by carbodiimide chemistry. The first method attempted was to conjugate amine-PEG-Folate to PLGA that had been precipitated as nanoparticles in an aqueous suspension. The efficiency of this reaction was hypothesized to be determined by the surface area of the nanoparticles, as well as the number of available carboxylic acid groups for activation. The second method was to perform the conjugation in anhydrous dichloromethane, in which PLGA is completely soluble. Though this reaction requires the use of an organic solvent, it was hypothesized that the

percent yield of PLGA-PEG-Folate would be greater due to complete dissolution of PLGA and availability of terminal carboxylic acid groups.
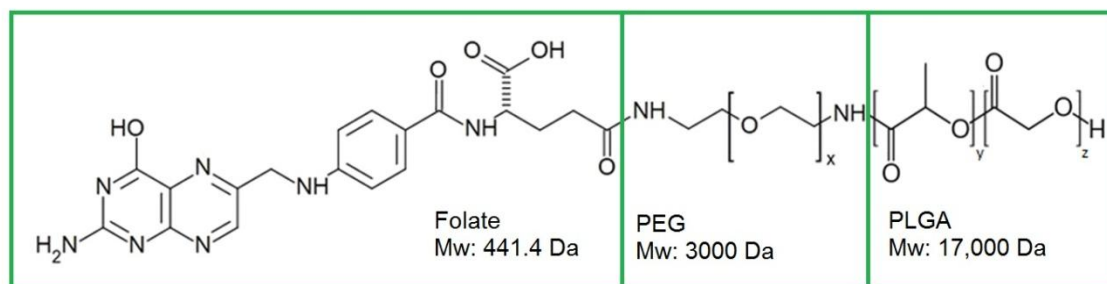
Figure 3.1. Structure of PLGA-PEG-Folate.

Carboxylic acid-terminated PLGA reacts with NH2-PEG-Folate by carbodiimide chemistry to give an amide bond. Folic acid is on the opposite side of PEG. The M.W. of the conjugate is approximately 21 kDa [72].

MATERIALS AND METHODS

Materials

Folic acid Polyethylene glycol amine (NH$_2$-PEG-Folate) was purchased from Nanocs (New York City, New York). Carboxylic acid-terminated poly(lactic-*co*-glycolic acid) (PURAC Purasorb® PDLG 5002A and 5004A, or PLGA) was purchased from

Corbion (Diemen, Netherlands). Poly(lactic-*co*-glycolic acid)-block-PEG (Resomer® RGPD 50105) was purchased from Evonik Industries (Essen, Germany). Polystyrene molecular weight standards were purchased from Alfa Aesar (Ward Hill, Massachusetts). DY-700 was purchased from Dyomics GmbH (Jena, Germany). Folic acid, dimethylsulfoxide (DMSO), tetrahydrofuran (THF), and triethylamine (TEA) were purchased from Fisher Scientific (Fair Lawn, New Jersey). Sodium bicarbonate was purchased from Sigma Aldrich (St. Louis, Missouri). 2-(*N*-morpholino)ethanesulfonic acid monohydrate (MES) was purchased from GenScript USA Inc. (Piscataway, New Jersey). 1-ethyl-3-(3-dimethylaminopropyl)carbodiimide hydrochloride (EDAC HCl) was purchased from AKSci (Union city, California). Glass wool, dichloromethane, N-hydroxysuccinimide, and sodium chloride were purchased from Acros Organics (Geel, Belgium). Dicyclohexylcarbodiimide (DCC) was purchased from Tokyo Chemical Industries (Tokyo, Japan).

Aqueous synthesis of PLGA-PEG-Folate

The first method of PLGA-PEG-Folate synthesis is in an aqueous nanosuspension. PLGA nanoparticles are first prepared by a modified solvent displacement method (Beck-Broichsitter). PLGA (PDLG 5002A, 17 kDa or PDLG 5004A, 40 kDa) was dissolved in 1 mL acetone at various concentrations, and precipitated into 5 mL water (pH adjusted to 5.0 with 0.1 M MES buffer) while stirring at 550 rpm. The acetone was left to evaporate for 4-6 hours while stirring at 850 RPM, after which EDAC HCl was added to the nanosuspension in a 2:1 molar ratio to PLGA. This solution was shaken at -20° C for 5 minutes. A solution of NHS dissolved in water was then added to the aqueous nanosuspension (2:1 molar ratio to PLGA) and the reaction was allowed to proceed for 2 hours. The pH of the nanosuspension was then slowly adjusted to between 8.0 and 8.5 by the use of 0.1 M bicarbonate buffer. NH_2-

PEG-Folate, dissolved in 0.1 M bicarbonate buffer, was then added to the surface-activated PLGA nanoparticles in a 2:1 molar ratio to PLGA. The conjugation proceeded at room temperature for 6. The product was purified by dialysis against deionized water at 4° C using Spectra/Por dialysis bags with an 8 kDa molecular weight cut off (Spectrum Laboratories, Rancho Dominguez, California) for 24 hours. The purified product was then lyophilized using a FreeZone 2.5 lyophilizer (LabConco, Kansas City, Missouri) and stored vacuum sealed at -20° C with a desiccant.

A

B
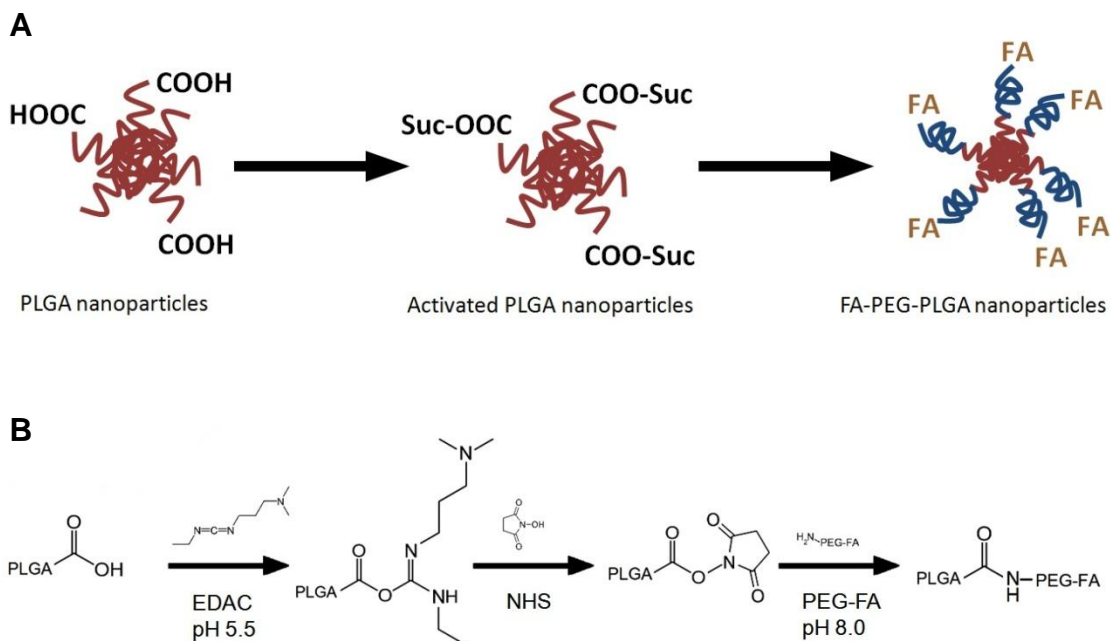
Figure 3.2. Reaction schemes for synthesis of PLGA-PEG-Folate in aqueous conditions.

(A) PLGA is precipitated and reacts with EDAC/NHS to give succinimide (Suc) groups that can react with the free amine of PEG-Folate. (B) Reaction results in formation of an amide bond between PLGA and PEG.

A

B
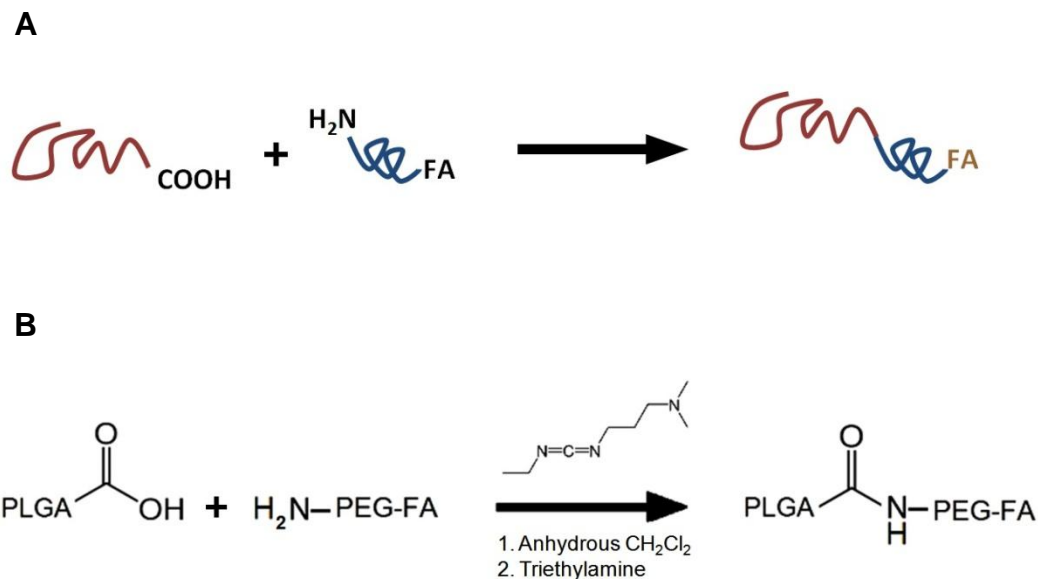
Figure 3.3. Reaction schemes for PLGA-PEG-Folate in dichloromethane.

(A) PLGA is completely solubilized, allowing easier access of carboxylic acid groups to the free amine of PEG-Folate. (B) After the acid catalyzed activation of carboxylic acid groups, triethylamine deprotonates the free amine of PEG-Folate to react with PLGA.

Organic synthesis of PLGA-PEG-Folate

The second method for synthesizing PLGA-PEG-Folate was performed by dissolving NH_2-PEG-Folate (4 mg) and carboxylic acid-terminated PLGA (10 mg, 2:1 molar ratio of PEG to PLGA) in 10 mL of dichloromethane that was made anhydrous with molecular sieves (1/16 inch pellets, Linde 3A, Strem Chemicals, Newburyport, Massachusetts). EDAC HCl was then added to the reaction (2:1 molar ratio to PLGA) and the solution was allowed to stir for 2 hours under positive pressure of nitrogen.

Following this step, triethylamine (100:1 molar ratio to PLGA) was added. The reaction was allowed to proceed for 48 hours. To purify the product, an aqueous extraction was performed using 50 mL of 1M NaCl, three times, to extract the excess PEG-FA and EDAC HCl (along with the urea byproduct of EDAC). The dichloromethane layer was then dried overnight at 4° C with molecular sieves. The next day, molecular sieves were filtered out, and the purified product was obtained by the evaporation of dichloromethane under a stream of nitrogen. The gel-like product was redissolved in THF and precipitated in water. The THF was allowed to evaporate, and then the suspension was lyophilized and vacuum sealed at -20° C with a desiccant.

Characterization of products

Molecular weights of the PLGA-PEG-Folate conjugates were confirmed by gel permeation chromatography using an HPLC system composed of a binary pump (1500-series HPLC pump, Waters, Milford, Massachusetts), a refractive index detector (2414 refractive index detector, Waters), and a Waters Styragel® GPC column (7.8 x 300 mm, 5 µm particle size, molecular weight range 50 Da-100 kDa, Waters). Refractive index detection works by comparing the refractive index of the sample solution to that of a pure solvent. The signal is given in millivolts (MV), which represents the amount of light hitting the photodiode as a result of refraction of incident light by the sample. The percent of PLGA conjugated to NH_2-PEG-Folate was determined by absorbance of folate at 365 nm using a µQuant microplate reader (BioTek, Winooski, Vermont).

For PLGA-PEG-Folate products synthesized by the aqueous reaction, Z-average particle size and polydispersity index values (PDI) were measured by dynamic light scattering using a Malvern high performance particle sizer (Malvern, UK), and zeta potential was measured by laser Doppler velocimetry using a Malvern Zetasizer

(Malvern, UK). These values were used to correlate particle size to efficiency of the conjugation, measured by folate absorbance.

Preparation of PLGA-PEG-Folate nanoparticles

Following conjugation of PLGA to NH_2-PEG-Folate, nanoparticles containing varying ratios of PLGA and PLGA-PEG-Folate were prepared by solvent displacement, as described previously. Ratios of PLGA-PEG-Folate copolymer were mixed with the PLGA homopolymer (20%, 40%, 65%, and 80% copolymer in PLGA) in acetone before precipitation in water. Following precipitation in water and evaporation of acetone (under hood on stir plate set to 850), nanosuspensions were lyophilized. Lyophilized products were vacuum sealed and stored at -20° C with a dessicant.

Differential scanning calorimetry of PLGA-PEG-Folate nanoparticles

Differential scanning calorimetry of lyophilized blank nanoparticles was conducted using a Q200 differential scanning calorimeter (TA Instruments, New Castle, Delaware) to see the effect of homopolymer (PLGA) solubility in copolymer (PLGA-PEG-Folate) on the glass transition temperature of the nanoparticle matrix. Lyophilized nanoparticles containing 20%, 40%, 65%, and 80% copolymer in PLGA were pressed in sealed aluminum hermetic pans for analysis by differential scanning calorimetry. Scans were conducted from 0° C to 300° C using a 10° C/min ramp rate. Glass transition temperatures were determined using the Universal analysis 2000 software package (TA instruments).

Folate content in PLGA-PEG-Folate conjugates

The first step in the conjugation of NH_2-PEG-Folate to PLGA using EDAC HCl is acid catalyzed. Specifically, protonation of the carbodiimide nitrogen on EDAC allows for the rearrangement of bonds required for the carboxylic acid group to bind to the carbodiimide carbon. The next step, however, requires deprotonation of the amine group on NH_2-PEG-Folate to bind the carbon of the carboxylic acid. This was achieved by changing the pH of the reaction solution in aqueous reactions and by the addition of an organic base, triethylamine, in reactions conducted in dichloromethane. Conjugation of NH_2-PEG-Folate to PLGA was successful in all reactions (**Table 3.1**). Folic acid concentration in products was measured by absorbance of folic acid at 405 nm by the plate reader, with both folic acid samples and polymer samples completely dissolved in DMSO to ensure there was no hindrance of measurement due to nanoprecipitated polymer.

Table 3.1.   Conjugation (%) of aqueous and organic reactions.

Aqueous reactions are divided into categories based on the original concentration of PLGA in acetone from which PLGA nanoparticles were precipitated.

Reaction			Conjugation
Aqueous	Mw 17 kDa	4 mg/mL	54 %
		6 mg/mL	38 %
		10 mg/mL	18 %
	Mw 40 kDa	10 mg/mL	25 %
Organic	Mw 17 kDa		65-81%

Effect of polymer molecular weight and particle size on efficiency of aqueous reaction

The conjugation of PLGA to NH_2-PEG-Folate following aqueous nanoprecipitation of PLGA was shown to be dependent on the PLGA and the particle size, but no correlation with molecular weight was seen. Four reactions, three with PLGA of molecular weight 17 kDa (PDLG 5002A) and one with a molecular weight of 40 kDa (PDLG 5004A), were performed.

Table 3.2. Conjugation efficiency as a result of polymer molecular weight and particle size.

Molecular weight of PLGA is given in the left most column, followed by the polymer concentration. Sizes of conjugates are typically a few nanometers larger than the original PLGA nanoparticles. Z-average size is given as the average of three measurements with standard deviation and does not indicate polydispersity. PDI, polydispersity index.

Sample			Z-average size (nm)	PDI	Conjugation (%)
PLGA 40 kDa	10 mg/mL	PLGA	136 ± 3	0.07 ± 0.00	-
		PLGA-PEG-FA	138 ± 1	0.07 ± 0.03	25
PLGA 17 kDa	4 mg/mL	PLGA	74 ± 0	0.17 ± 0.02	-
		PLGA-PEG-FA	81 ± 0	0.13 ± 0.01	54
	6 mg/mL	PLGA	81 ± 0	0.14 ± 0.03	-
		PLGA-PEG-FA	94 ± 2	0.18 ± 0.06	38
	10 mg/mL	PLGA	105 ± 2	0.15 ± 0.02	-
		PLGA-PEG-FA	107 ± 1	0.15 ± 0.02	18

It is known (and shown here) that preparing PLGA nanoparticles by modified solvent displacement from a lower polymer concentration in acetone results in smaller particles [53]. The three reactions with PLGA of molecular weight 17 kDa were used to

determine the effect of this change in particle size on the efficiency of the reaction. We hypothesized that smaller particles would result in greater conjugation efficiency, due to increased surface area per unit mass. This means that the number of carboxylic groups available for reaction is likely to be greater. We showed that, indeed, lower PLGA particle sizes resulted in greater conjugation efficiency.

Physicochemical characterization of the PLGA particles before and after conjugation with NH2-PEG-Folate was also performed (Table 3.2). We show that in all cases, particle size of the conjugate is higher than the parent PLGA particles. Additionally, we show that a greater change in the particle diameter resulted with those particles that had higher conjugation efficiencies.

Gel permeation chromatography

Gel permeation chromatography, or GPC, was chosen as another method to confirm the conjugation by determining the molecular weight of the conjugates, compared to the initial products. GPC is a type of size-exclusion chromatography, where resolution of compounds occurs by retention in pores as a function of molecular weight, as opposed to hydrophilic or hydrophobic interaction with the stationary phase. Parameters calculated by the Empower® software (Waters) include the number average molecular weight (M_n), the mass average molecular weight (M_w), and the molecular weight at the sample peak maximum (M_p).

M_n is calculated as the average molecular weight of all species in a particular sample. This is calculated by the following equation:

$$M_n = \frac{\sum N_i M_i}{\sum N_i}$$

where M_i is the molecular weight of a given species and N_i is the number of that species present in the sample.

Mw is the mass average molecular weight of all species in a sample, and is calculated as follows:

$$M_w = \frac{\sum N_i M_i^2}{\sum N_i M_i}$$

In this equation, each component of both sums (numerator and denominator) is multiplied by the M_i of that component. This weights the calculated molecular weight towards heavier species (and is therefore always larger than M_n). Polydispersity is calculated as the ratio of M_w to M_n and is always greater than 1. Lower polydispersity indicates a narrower molecular weight distribution.

The molecular weight (M_p) for PLGA before conjugation, as measured by GPC, was approximately 16 kDa, in agreement with the value given by the manufacturer. The expected molecular weight of all products was approximately 21 kDa, which is the theoretical molecular weight of the conjugate. For the reactions conducted in an aqueous suspension, conjugation percentages measured by the plate reader were between 18% and 54%. Following GPC analysis of these conjugates, it is clear that the predominant polymers measured in these reactions are the original reactants, i.e. unconjugated PLGA and NH_2-PEG-Folate. However, reactions performed in dichloromethane generated products much closer to the anticipated molecular weight, i.e. 21 kDa. This further indicates that high conjugation and reaction yields require more availability of carboxylic acid groups. Examples of gel permeation chromatograms are shown in **Figures 3.5 and 3.6**.
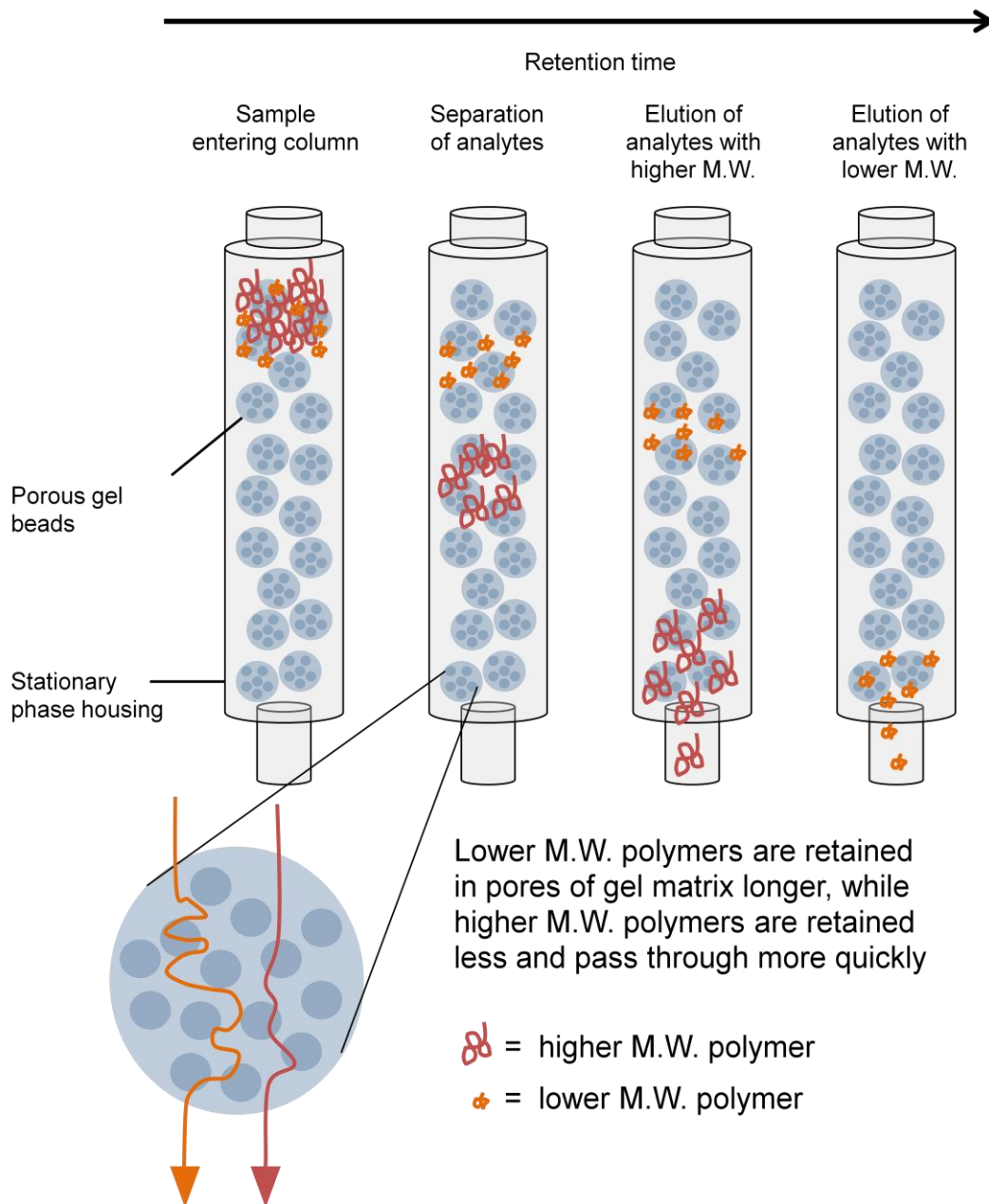
Figure 3.4. Gel permeation chromatography theory.

Gel permeation chromatography works by separating molecules of different molecular weights using a porous gel matrix. Lighter compounds reside in pores for longer and therefore elute later than larger, heavier compounds.

Table 3.3. Polystyrene molecular weight standards.

Molecular weights, retention times, and polydispersity indices of polystyrene molecular weight standards. The range of standards chosen is sufficient to approximate the molecular weight of the product conjugation of PLGA to PEG-Folate. Polydispersity values were very low. MW, molecular weight; RT, retention time.

RT (min)	MW	Log_{10}(MW)	Polydispersity
6.95	50000	4.69	1.06
7.36	25000	4.39	1.06
7.72	13000	4.11	1.06
8.21	5200	3.71	1.06

Table 3.4. Retention times and molecular weights of conjugation products.

Molecular weights are calculated according to the calibration curve in the Appendix (A.1). Percent area refers to the relative percent of areas of all components of the product peaks analyzed.

Sample name		RT (min)	M_n (Da)	M_w (Da)	M_P (Da)	Polydispersity	% Area
Organic reaction solution		7.42	13935	21879	21932	1.57	100
Aqueous reaction solution	Peak 1	7.57	12399	18779	16773	1.51	96.06
	Peak 2	8.59	2479	2571	3681	1.04	3.94
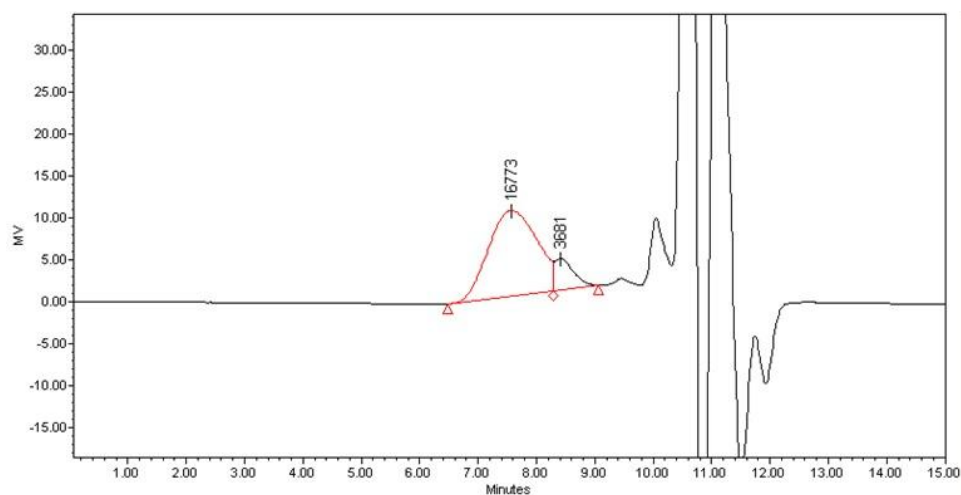
Figure 3.5. Chromatogram of the product of an aqueous reaction.

Predominant peaks are approximately 17 kDa (most likely PLGA) and 3.4 kDa (most likely PEG-folate). MV, millivolts.
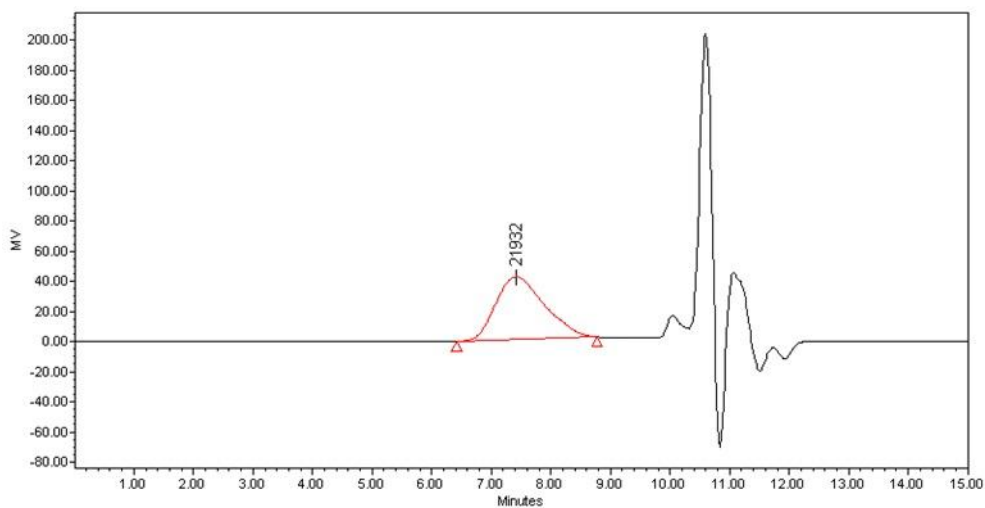
Figure 3.6. Chromatogram of a product from a reaction performed in dichloromethane.

M_p of the predominant compound is approximately 21 kDa, which is expected for PLGA-PEG-Folate. MV, millivolts.

Glass transition temperature following conjugation of NH$_2$-PEG-Folate to PLGA

Differential scanning calorimetry of nanoparticles composed of varying ratios of the block copolymer, PLGA-PEG-Folate, to PLGA, was conducted to determine the thermal properties of nanoparticles composed of polymers in these ratios. Glass transition temperatures are shown in **Table 3.4**. It is evident that the glass transition temperatures are shifting lower as a result of the presence of the copolymer in the PLGA matrix. The presence of PLGA-PEG-Folate causes more plasticity of the PLGA matrix and disrupts the crystal structure of the PLGA. This phenomenon has been noted before with different polymer/copolymer matrices, where the transition temperature decreases as a result of the introduction of a copolymer in the matrix [73]. This is encouraging for us because it shows that the two polymers are miscible within one another at these ratios. The lowering glass transition temperatures are plotted in **Figure 3.7**. It seems that there is a point at which the T$_g$ shifts rapidly to a lower temperature, which might reflect changes in the crystal morphology of the polymer matrix when the copolymer is added. Lower ratios are much closer to the original T$_g$ of the PLGA, while higher ratios result in substantial change in the crystal structure. Curiously, 20% PLGA-PEG-Folate in PLGA exhibited another distinct glass transition temperature at 58.77° C. This is most likely a reflection of a very well-known phenomenon whereby miscible polymers can have two glass transitions due to variations in local composition and crystallinity within the matrix. Heterogeneity within the matrix can theoretically cause certain regions to have different thermal properties from other regions. This phenomenon is not present in the other ratios, likely meaning that higher PLGA-PEG-Folate concentrations reduce heterogeneity within the polymer matrix [74].

Table 3.5. Glass transition temperatures of nanoprecipitated polymer/copolymer blends.

Glass transition temperatures of nanoprecipitated polymer/copolymer (PLGA/PLGA-PEG-Folate) matrices at different ratios, compared to non-nanoprecipitated PLGA. "X" refers to the weight ratio of the PLGA-PEG-Folate to the PLGA, given in percent.

Sample	X %	T_g (°C)
PLGA (17 kDa, non-nanoprecipitated)	0	44.05
	20	42.89, 58.77
PLGA + **X %** PLGA-PEG-Folate (nanoparticles)	40	42.69
	65	32.14
	80	31.47
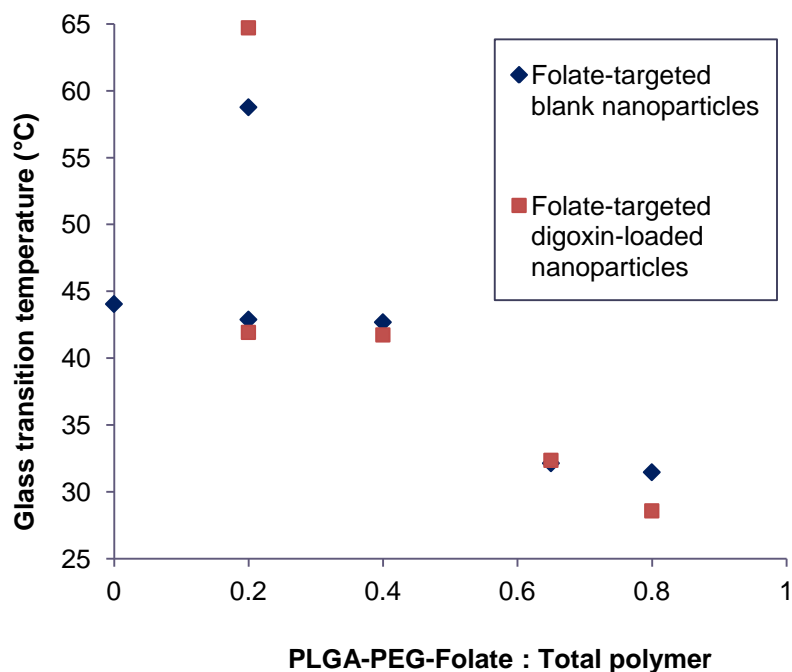
Figure 3.7. Glass transition temperatures of nanoprecipitated polymer/copolymer blends.

Plot of the shift in glass transition temperatures of the nanoprecipitated polymer/copolymer matrix when PLGA-PEG-Folate (block copolymer) is mixed with PLGA (polymer) in different ratios. 80% is the maximum conjugation that was achieved. Other concentrations represent purified product (80%) diluted into PLGA. There is a drastic shift between 40% and 65% block copolymer in the polymer matrix.
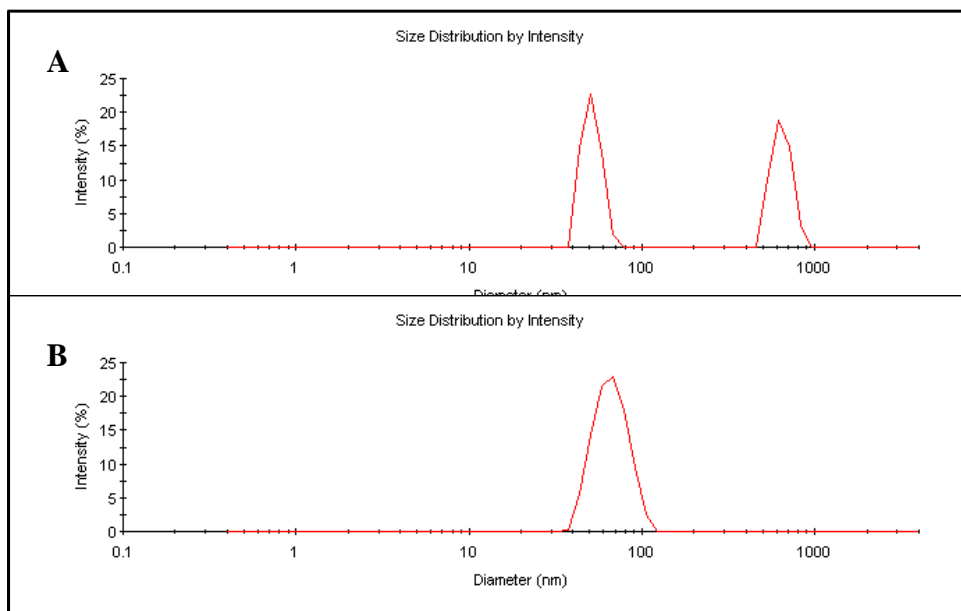
Figure 3.8. Size distribution graphs of nanoparticles.

Size distributions, measured by high performance particle sizer, are shown of nanoparticles made of (A) 20% PLGA-PEG-Folate and 80% PLGA and (B) 80% PLGA-PEG-Folate and 20% PLGA.

CONCLUSION

Folate functionalized polymers were prepared by carbodiimide chemistry. Folate, present on the opposite terminus of the hydrophilic PEG block to the PLGA, should be available on the surface of nanoparticles precipitated in water, allowing for interaction with folate receptors of the placenta. The hydrophobic nature of PLGA, on the other hand, should cause it to remain on the inside of nanoparticles and encapsulate digoxin within its matrix. The efficiency of the reaction linking NH$_2$-PEG-Folate to PLGA is

largely dependent on the availability of carboxylic acid termini of PLGA. We show that, for reactions conducted in aqueous nanosuspensions, there is a clear correlation between smaller particle size and increased conjugation efficiency.   Further, conjugation efficiency is increased when PLGA is completely dissolved in dichloromethane. Differential scanning calorimetry of various ratios of the copolymer in the polymer matrix shows that the polymers are indeed miscible, as can be seen by the shift in the glass transition temperature.   This conjugated product, PLGA-PEG-Folate, can theoretically be used to encapsulate digoxin and allow transplacental transport across BeWo cells.

Chapter 4: Comparison of digoxin loaded folate-targeted and non-targeted nanoparticle transport in *in vitro* placental model

INTRODUCTION

The focus of this chapter is to test the ability of nanoparticles containing folic acid on the surface to target the placenta and increase endocytosis, leading to increased delivery of digoxin to the fetal compartment. As described in the previous chapter, folate receptors present on the placenta may increase the transplacental transfer of digoxin loaded nanoparticles by folate receptor-mediated endocytosis, a well known phenomenon studied in numerous tissue types [75]. The advantage of this type of endocytosis is that during pregnancy, folate receptors are expressed in relatively high quantities in the placental trophoblast. These are necessary for the uptake of folic acid by the fetus for many functions, the most widely known of which is the development of the neural tube. Neural tube defects, including spina bifida, may be the result of folic acid deficiency during pregnancy, and many cases can be avoided by folic acid supplementation [41].

This project seeks to exploit the presence of folic acid receptors in delivering digoxin to the fetal compartment (**Figure 4.1**). Folic acid receptors, especially necessary during the first few weeks of gestation, are expressed by the placenta throughout pregnancy [67]. The time at which preliminary investigations of congenital heart disease occurs is typically around 18-22 weeks, and in many cases fetal arrhythmias are not detected until the early third trimester [4]. Since folic acid may interact with receptors and therefore inhibit some endocytosis of folate-functionalized nanoparticles, it would be feasible to stop folate supplementation for the purpose of targeted placental delivery of digoxin.
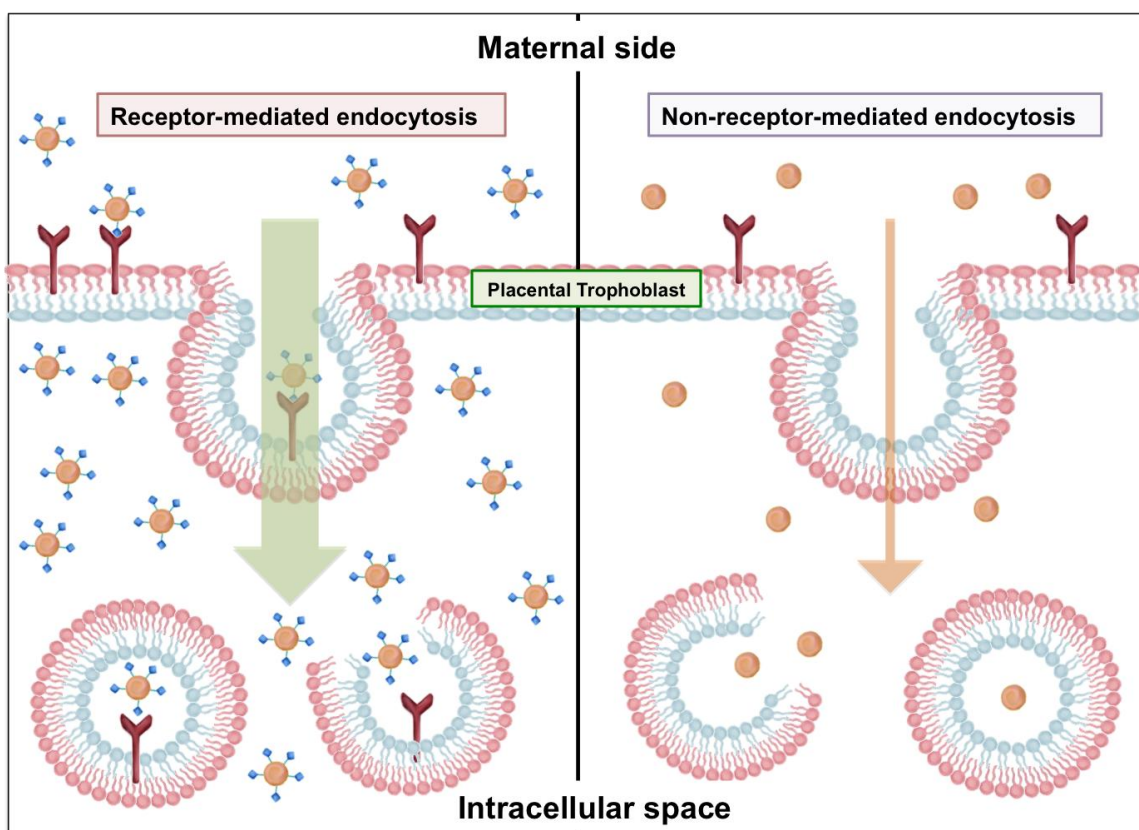
Figure 4.1. Folate receptor mediated endocytosis.

Folate molecules on the surface of nanoparticles can increase endocytosis into cells, increasing delivery to folate receptor-expressing tissues.

Folate-targeted digoxin loaded nanoparticles were prepared from PLGA-PEG-Folate, as described in the previous chapter. Digoxin was loaded into nanoprecipitated PLGA-PEG-Folate, and the effect of folic acid targeting was investigated in BeWo cell transport studies (similar to chapter 2). Digoxin loading in PLGA-PEG-Folate and blends of PLGA-PEG-Folate with PLGA were further examined by differential scanning calorimetry.

Additionally, we covalently attached a fluorescent dye, DY-700, to carboxylic acid-terminated PLGA for the purposes of loading it in folate-targeted nanoparticles for *in vivo* tracking of targeted nanoparticles. DY-700 is a fluorescent dye with excitation and emission in the near infrared range, thus limiting interference from tissue autofluorescence and increasing sensitivity. This fluorophore tagged polymer was then loaded into PLGA nanoparticles to determine the feasibility of detecting low nanoparticle concentrations by an *in vivo* imaging system.

MATERIALS AND METHODS

Materials

PLGA-PEG-Folate was prepared according to the process described in Chapter 3. Carboxylic acid-terminated poly(lactic-co-glycolic acid) (PURAC Purasorb® PDLG 5002A and 5004A) was purchased from Corbion (Diemen, Netherlands). DY-700 was purchased from Dyomics GmbH (Jena, Germany). Glass wool, dichloromethane, N-hydroxysuccinimide, and sodium chloride were purchased from Acros Organics (Geel, Belgium). Dicyclohexylcarbodiimide (DCC) was purchased from Tokyo Chemical Industries (Tokyo, Japan).

Preparation of digoxin-loaded folate-targeted nanoparticles

Products from synthesis of PLGA-PEG-Folate were used to prepare digoxin-loaded folate-targeted nanoparticles by a modified solvent displacement method. PLGA-PEG-Folate with 65% conjugation (3 mg/mL) and digoxin (0.333 mg/mL, for 10% drug

loading) were dissolved in tetrahydrofuran. For the preparation of non-targeted nanoparticles, 65% PEG-PLGA and 35% PLGA were used to approximate the amount of PEG present in targeted nanoparticles. Percent drug loading was held constant and polymer concentrations of 2, 3, and 5 mg/mL were prepared to compare to targeted nanoparticles. Blank nanoparticles were also prepared using 2, 3, and 5 mg/mL of 65% PEG-PLGA and 35% PLGA in THF. Of the polymer or polymer/digoxin solution, 1 mL was precipitated in 5 mL of deionized water at a rate of 6.0 mL/min using a variable-speed peristaltic pump (Traceable® Calibration Control Company, Friendswood, TX) through a 22 gauge needle (0.7mm x 40mm, PrecisionGlide Needle®, BD, Franklin Lakes, NJ), while stirring at 550 RPM. The nanosuspension was then left stirring at 850 RPM in the hood for approximately 8 hours to allow all of the THF to evaporate. The final volume of the nanosuspension was completed to 5 mL of deionized water and stored at 4° C.

High performance liquid chromatography

HPLC analysis of digoxin concentrations in cell culture media was performed as described in chapter 2, with slight modifications. Flow was established using a binary pump (1500-series HPLC pump, Waters, Milford, Massachusetts) at 1 mL/min under isocratic conditions of 60:40 (v/v) purified water to acetonitrile, using a Kromasil ® C-18 column (AkzoNobel Separation Products, Bohus, Sweden). The column was heated to 30° C.

Samples in media were prepared by precipitating 100 µL of DMEM/F-12 media (Dulbecco's Modified Eagle's Medium/Ham's F-12 50/50 mixture, Mediatech, Manassas, VA) containing digoxin in 400 µL of acetonitrile and centrifuging the solution at 15,000 rcf at room temperature for 15 minutes in an Eppendorf® 5430 centrifuge (Hamburg, Germany) to pellet all precipitated proteins. Of the supernatant, 450 µL was

removed and placed in a glass vial. This solution was allowed to dry under a controlled nitrogen stream using a ZipVap24 ® (Glas-Col LLC, Terre Haute, Indiana). After the sample was dry, the residue was reconstituted in 120 µL the mobile phase mixture. Of the reconstituted residue, 100 µL was injected into the HPLC system. Detection was achieved by UV absorbance (230 nm) using a Waters 2998 photodiode array detector (Milford, MA). This method was partially revalidated for accuracy, precision, and linearity in the necessary concentration ranges for the transport study.

Nanoparticle characterization

The size and zeta potential of nanoparticles were determined prior to *in vitro* transport studies. Polydispersity indices and diameter of nanoparticle formulations were determined by dynamic light scattering (High performance particle sizer, Malvern Instruments, Malvern, UK). The size non-targeted nanoparticles (digoxin loaded and blank, precipitated from 2, 3, and 5 mg/mL solutions of polymer in THF) were screened to match digoxin-loaded targeted nanoparticles. Additionally, zeta potential of nanoparticles was determined by laser Doppler velocimetry (ZetaSizer, Malvern Instruments, Malvern, UK).

Glass transition temperatures of digoxin-loaded folate targeted nanoparticles with varying ratios of PLGA to PLGA-PEG-Folate were measured using a Q200 differential scanning calorimeter (TA Instruments, New Castle, Delaware). Nanoparticle suspensions were lyophilized using a FreeZone 2.5L benchtop freeze dry system (Labconco, Kansas City, Missouri) and subsequently pressed in sealed aluminum hermetic sample pans. Thermal properties were determined by measuring heat flow while scanning from 0° C to 300° C at a rate of 10° C/min.

Cell culture

Cell culture was performed similarly to Chapter 2. Briefly, BeWo (b30 clone) cells were cultured in DMEM/F-12 media containing 10% fetal bovine serum containing 10,000 units/mL penicillin 10,000 μg/mL streptomycin, and 25 μg/mL amphoterecin B, 100X non-essential amino acid solution, and 100 mM L-glutamine. Cells were revived from stocks stored in liquid nitrogen (passage 27), and grown in a 95% humidified incubator with 5% CO_2 at 37° C. At confluence (80-90%), cells were seeded on polycarbonate Transwell inserts at a density of 224,000 cells/mL. Transwells were coated with human placental collagen prior to seeding, as described previously. Cell culture media was changed every day, and transepithelial electrical resistance (TEER) was measured using an EndOhm® voltohmmeter (World Precision Instruments, Sarasota, Florida). Cells were grown until TEER values were between 30 and 60 $\Omega \cdot cm^2$. Transwells were distributed between experimental groups so that each group had similar TEER values.

Transport studies

Transport studies were conducted on seeded transwell plates that had reached appropriate TEER values, similar to the protocol described in chapter 2. Briefly, 0.5 mL of media containing each treatment was added to the apical side of the Transwell inserts, while the basolateral side received 1.5 mL of blank media. Treatment groups included free digoxin, free digoxin and blank polymeric nanoparticles, digoxin-loaded polymeric nanoparticles, folate-targeted digoxin-loaded nanoparticles, and folate-targeted digoxin-loaded nanoparticles in the presence of 5 μM folic acid. Folic acid was used as a competitive inhibitor at the folate receptor of BeWo cells. Inserts were maintained in the same incubation conditions for the duration of the study. Samples and prespecified time

points were taken from basolateral chamber and analyzed according to the HPLC method described above. From these, mass transfer and apparent permeability of digoxin was calculated (similar to chapter 2).

Conjugation of DY-700 to PLGA

DY-PLGA was prepared in a manner that is similar to a method described previously [76]. Briefly, DY-PLGA was prepared by first dissolving 50 mg of carboxylic acid terminated PLGA (PDLG 5002A) and DCC (2:1 molar ratio to PLGA) in dichloromethane that had been dried over molecular sieves. The reaction solution was allowed to stir for 10 minutes, after which NHS (2:1 molar ratio to PLGA), dissolved in dichloromethane, was added to the reaction. The reaction was monitored for the presence of a white precipitate, dicyclohexylurea (DCU). After the appearance of the precipitate, the solution was allowed to stir for an additional 2 hours. The crude reaction mixture containing activated PLGA was then passed through a short column packed with glass wool to remove DCU precipitate. A clear solution of NHS-PLGA was obtained and used for the conjugation with DY-700.

DY-700 (1 mg) was dissolved in anhydrous dichloromethane (protected from light). To this solution, 23 mg (equimolar amount to DY-700) of activated PLGA was added. The reaction was allowed to stir at room temperature for 16 hours. The reaction solution was then precipitated in ice cold methanol (10:1 volume ratio to dichloromethane). The precipitate was distributed in centrifuge tubes and centrifuged at 4° C at 13,200 rcf for 2 hours in an Eppendorf 5415 R centrifuge (Eppendorf, Hamburg, Germany). The supernatant was discarded and the pellets were collected and washed with ice cold methanol three times. The product was then dried under a nitrogen stream and stored at -20° C with a desiccant.

Figure 4.2. Conjugation of PLGA to DY-700.

PLGA is activated by DCC, followed by NHS. DY-700 contains an amine group which reacts with the activated carboxylic acid group of PLGA.

Preparation of fluorescent polymeric nanoparticles

Fluorescent nanoparticles were prepared by co-precipitating DY-PLGA with PLGA (17 kDa). Briefly, PLGA (2.65 mg) and DY-PLGA (0.35 mg) were mixed in acetone (1 mL) to give 0.5% dye loading by mass. This solution was precipitated in 5 mL of deionized water by addition with a peristaltic syringe pump, while stirring at 550 rpm (previously described). The acetone was allowed to evaporate while stirring at 850 rpm. Following evaporation of acetone, the nanoparticles were used to create a dilution series in water and placed in a 96 well plate for imaging in an IVIS Spectrum (Perkin Elmer, Waltham, Massachusetts).

Characterization of fluorescent nanoparticles

DY-700 has an absorption maximum at 707 nm and a maximum emission wavelength of 730 nanometers. Concentrations of DY-700 bound to PLGA (precipitated in PLGA nanoparticles) were measured using an In Vivo Imaging System (IVIS Spectrum). Briefly, a nanoparticle dilution series was pipeted into a black-walled 96 well

plate (clear bottom) for fluorescence measurements. The plate was placed in the imaging chamber. Filters for absorption (675 nm) and emission (740 nm) were set to maximize fluorescent signal. The IVIS system was allowed to autocalibrate to reduce noise.

Statistical analysis

For the HPLC method, a standard curve using 1/X weighting was prepared using SigmaPlot v. 12.5 (Systat software Inc, Chicago, Illinois). Averages and standard deviations of peak areas were calculated, as well as deviation from the linear regression. Averages and standard deviations were calculated for each experimental group in an experiment, including cytotoxicity and permeability. Data were analyzed using the Student's t-test between designated groups, with a p-value less than 0.05 considered a significant difference. One-way analysis of variance test was conducted to determine if there were any significant differences between all groups.

RESULTS AND DISCUSSION

High performance liquid chromatography

The HPLC method was partially revalidated due to changes in sample preparation. Media samples were added to acetonitrile to precipitate proteins in the media from the addition of fetal bovine serum. This was done to prevent accumulation of protein in the C-18 column and prevent backpressure fluctuations in the binary pump. This method was highly sensitive and specific, and a linear correlation between digoxin concentration and peak area was seen (Appendix A.3).

Physicochemical characteristics of nanoparticles

Nanoparticles, prepared by a modified solvent displacement method, were characterized by dynamic light scattering and laser Doppler velocimetry. Non-targeted nanoparticles were prepared from 2, 3, and 5 mg/mL polymer solutions dissolved in THF, with and without 10% digoxin loading. Similarly, targeted nanoparticles containing 10% digoxin loading were prepared from 3 mg/mL of polymer (PLGA : PLGA-PEG-Folate 35:65, as synthesized). The sizes and zeta potentials of these nanoparticles are given in **Table 4.1**. Nanosuspensions with the most comparable size to the folate-targeted digoxin-loaded nanoparticles were the non-targeted digoxin-loaded nanoparticles prepared from 3 mg/mL polymer in THF and the non-targeted blank nanoparticles prepared from 2 mg/mL polymer in THF (highlighted in **Table 4.1**). Zeta potentials of these nanoparticles were also very similar.

Table 4.1. Nanoparticle screening for transport study.

All nanoparticles were loaded with 10% digoxin, unless indicated as "blank." Nanoparticles were chosen based on similar size and zeta potential.

Formulation	Z-average particle size (nm)	Polydispersity
Targeted nanoparticles	137 ± 1	0.13 ± 0.01
Blank nanoparticles	125 ± 1	0.16 ± 0.01
Non-targeted nanoparticles	116 ± 3	0.13 ± 0.01

Differential scanning calorimetry revealed interesting thermal properties regarding the ratio of PLGA to PLGA-PEG-Folate, and its ability to encapsulate digoxin. As shown in TABLE, the glass transition temperature of the 80% PLGA-PEG-Folate digoxin-loaded nanoparticles went down from the original 80% PLGA-PEG-Folate blank nanoparticles, indicating encapsulation at this ratio. However, the 20% PLGA-PEG-Folate nanoparticles that were loaded with digoxin still exhibited the characteristic two glass transition temperatures of the blank nanoparticles. This indicated that encapsulation probably did not occur at this ratio, and that the digoxin-loaded nanoparticles, like the blank nanoparticles, had a more segmented crystallization pattern (see chapter 3, page 57, for additional details). Interestingly, particle size when measured by dynamic light scattering of the 20% PLGA-PEG-Folate nanoparticles showed two distinct peaks, likely representing two distinct types of nanoparticles present in the suspension (**Table 4.1**). This is in agreement with the thermograms that showed two glass transition temperatures, indicating that the polymers are precipitating separately. The reason for this may be that the PEG in PLGA-PEG-Folate makes the entire polymer more water soluble, whereas unconjugated PLGA is less soluble in water and thus precipitates differently, yielding a sample with two different particle size peaks by dynamic light scattering.

Table 4.2.   Glass transition temperatures and peak areas of nanoparticle samples.

PLGA containing 20% PLGA-PEG-Folate has two glass transition temperatures and two predominant size distribution peaks, whereas PLGA containing 80% PLGA-PEG-Folate has one glass transition temperature and one predominant peak.

Sample	T_g (°C)	Z-average size (nm)	Peak 1 size (nm)	Peak 1 %	Peak 2 size (nm)	Peak 2 %
PLGA + 20% PLGA-PEG-Folate	41.93, 64.71	103 ± 1	163 ± 39	73 ± 21	44 ± 32	27 ± 21
PLGA + 80% PLGA-PEG-Folate	28.58	85 ± 1	93 ± 11	97 ± 4	5061 ± 4383	2 ± 3

Transport studies

Transport studies were conducted with cells seeded on human placental collagen coated polycarbonate Transwell inserts. The average TEER values of the experimental groups were between 62.7 and 66.1 $\Omega \cdot cm^2$. Transport across BeWo cells was measured by calculation of permeability, as described above.

Permeability measurements showed that nanoparticles containing folic acid groups on the surface increased nanoparticle endocytosis by folate receptor-mediated endocytosis. Digoxin-loaded nanoparticles containing folic acid on the surface had significantly higher permeability ($9.44 \times 10^{-6} \pm 1.86 \times 10^{-6}$ cm/s) than free digoxin ($3.66 \times 10^{-6} \pm 1.07 \times 10^{-6}$ cm/s), confirming that these nanoparticles can increase the ability of

digoxin to cross the cell membrane. There are two distinct mechanisms causing this phenomenon. First, PLGA-PEG nanoparticles can shield digoxin from P-gp efflux, as shown in Chapter 2. However, these nanoparticles are also able to bind folic acid receptors and participate in folate receptor-mediated endocytosis. This was tested by treating the apical side of placental trophoblast cells with targeted nanoparticles and free folic acid (5 μM). Folic acid in the apical chamber competes with the targeted nanoparticles for folate receptors, and reduced digoxin permeability from $9.44 \times 10^{-6} \pm 1.86 \times 10^{-6}$ cm/s to $5.04 \times 10^{-6} \pm 1.36 \times 10^{-6}$ cm/s. Inhibition of nanoparticle transport in the presence of excess folic acid is evidence that folate receptor-mediated endocytosis is a major mechanism by which targeted nanoparticles are able to cross the placental trophoblast.

It should be noted that two other groups were tested, namely non-targeted digoxin-loaded nanoparticles, and free digoxin in the presence of blank nanoparticles. Due to high variability in digoxin permeability of these treatment groups, no conclusions could be drawn. However, it was already previously shown that non-targeted digoxin-loaded nanoparticles increase digoxin permeability by shielding from P-gp, and that blank nanoparticles demonstrate no cytotoxicity in the concentrations used in this experiment (Chapter 2). Permeabilities, as well as relative standard deviations of all treatment groups, are shown in the appendix.
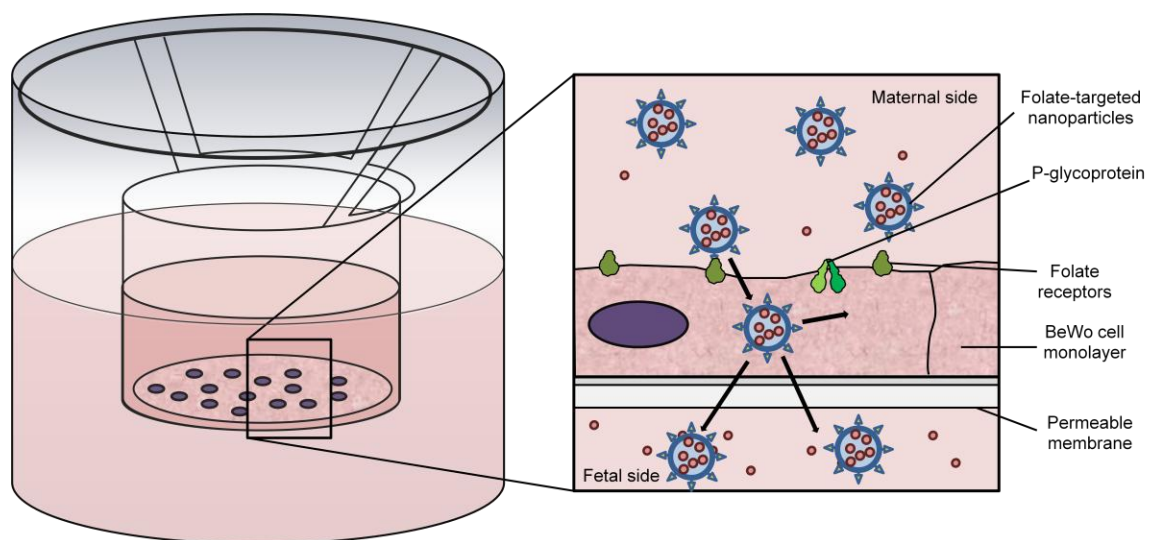
Figure 4.3. Folate receptor targeted transport study.

Folate receptor-mediated endocytosis of digoxin-loaded PLGA-PEG nanoparticles in BeWo cells.
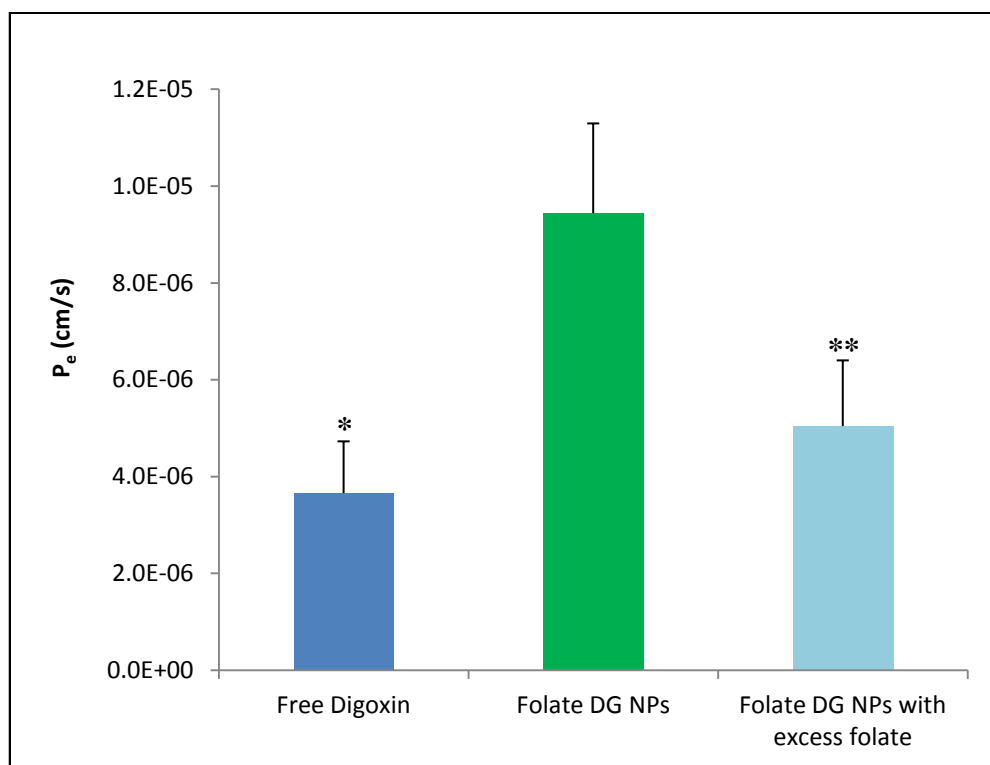
Figure 4.4. Apparent permeability (P_e) of digoxin in targeted nanoparticles.

Apparent permeability (P_e) values for digoxin loaded in folate-targeted nanoparticles across BeWo cells at 2 hours. Excess folate was used to inhibit folate receptor-mediated endocytosis. Significant differences were determined using ANOVA. (*, $p<0.001$ compared to folate DG NPs; **, $p=0.001$ compared to folate DG NPs) DG, Digoxin. NPs, nanoparticles.

Characterization of fluorescent nanoparticles

Conjugation of DY-700 to PLGA (PDLG 5002A) yielded a dark green solid that was insoluble in ice-cold methanol. After washing to remove excess dye, the mass yield

of the product was 11.5 mg, or approximately 50%. This product was loaded into folate-targeted and non-targeted nanoparticles with 0.5% DY-700 loading by mass. Covalent attachment of the fluorophore is superior to non-covalent loading because much less drug release would theoretically occur from the nanoparticle, allowing *in vivo* tracking of nanoparticles without mistakenly tracking free dye. The concentration dependence of the signal from IVIS was shown as a proof of principle that the nanoparticles can be detected *in vivo* with high sensitivity. Linear fluorescence detection of DY-700 functionalized PLGA nanoparticles was possible at a concentration of 187.5 ng/mL, or 251 nM (MW_{DY-700} = 747.4 Da). Similar concentrations for *in vivo* studies are expected to give a detectable signal. Based on the dose of nanoparticles administered, the dye loading of nanoparticles can be adjusted to visualize our minimum requirement for a detectable concentration for tissue accumulation analysis.

Figure 4.5. Near IR fluorescence of nanoparticles in 96 well plate by IVIS.

DY-700 loaded nanoparticles (0.5% dye loading) were placed in a 96 well plate. Noise level was set to 600 counts. Samples were loaded in rows B-G, columns 3-8.

CONCLUSION

It is evident that folate targeted digoxin-loaded nanoparticles are capable of increasing permeability of digoxin across the placental trophoblast. This is most likely due to two distinct phenomena, i.e., shielding from P-gp efflux and folate receptor-mediated endocytosis.
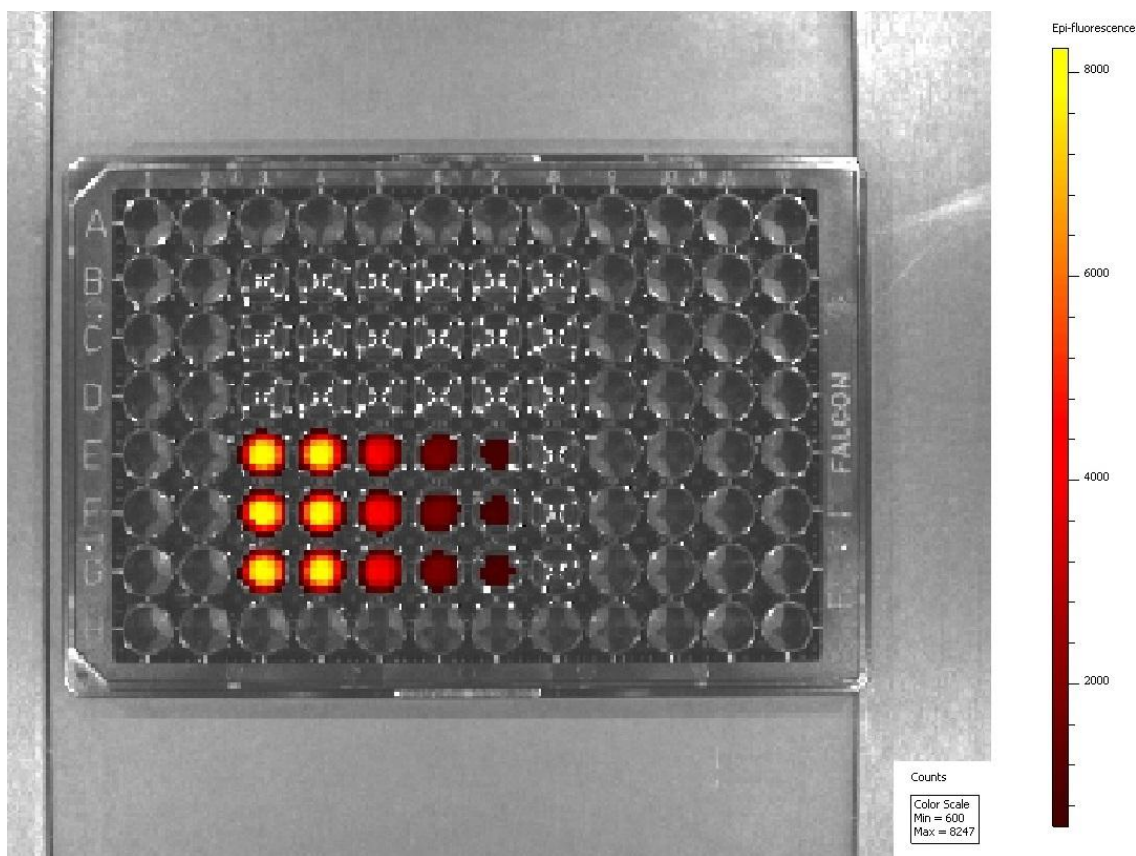
Important to consider is maternal administration of folic acid as a prenatal supplement. However, the time at which folic acid supplement is crucial is before and during the development of the fetal neural tube. The neural tube closes by the fourth week of gestation. The fetal heart typically begins beating at this time, but preliminary screening of congenital heart defects by echocardiogram is usually done at 18-22 weeks, and many fetal arrhythmias are not detectable until the late second or third trimester [4]. Though folate supplementation is essential before pregnancy and early in the first trimester, there is no evidence that it is necessary after the first trimester [77]. Therefore, the high folic acid doses given during the first trimester could be temporarily ceased in the case of administration of folate receptor-targeted digoxin-loaded nanoparticles.

Exploitation of folate receptors in the placental trophoblast is a novel approach to selective delivery of pharmaceuticals to the fetus. This is particularly important in cases of pharmacotherapy in which maternal administration of a drug for transplacental delivery can severely impair the health of the mother. Digoxin is one of the compounds that, though necessary in cases of fetal tachyarrhythmia, remains in the maternal circulation and can cause severe toxicity. These nanoparticles, therefore, present a promising and clinically feasible solution to problems associated with transplacental or intracordal digoxin treatment for fetal tachyarrythmias.

In addition, we prepared PLGA functionalized with a near infrared dye, DY-700. Covalent conjugation of DY-700 to PLGA will allow it to remain within the nanoparticle matrix and only be released upon hydrolysis of the polymer, allowing for tracking of the

nanoparticle *in vivo* and determining the sites of accumulation. These particles have been imaged using an *in vivo* imaging system. Folate-functionalized nanoparticles containing DY-700 can be used in future studies *in vivo* in pregnant rats to determine the degree of accumulation in placental and fetal tissue, compared to non-targeted nanoparticles.

Chapter 5: Conclusions

SUMMARY AND CONCLUSIONS

Transport of digoxin-loaded polymeric nanoparticles across BeWo cells, an *in vitro* model of human placental trophoblast

This chapter contained our preliminary investigation of the ability to load digoxin into biodegradable PLGA-PEG nanoparticles. We were able to screen nanoformulations for optimal physicochemical characteristics and drug loading. Most formulations had sufficiently high encapsulation efficiency, and due to previous research suggesting that polymeric nanoparticles cross the placental trophoblast in a size dependent manner, we selected the smallest particles for our studies. We were able to show, by differential scanning calorimetry, that digoxin was incorporated into the crystalline matrix of the polymer, reducing the glass transition temperature. These particles exhibited sustained release that fit the Higuchi model for controlled drug release out of a spherical matrix.

Our most important finding detailed in this study was that these polymeric nanoparticles were able to cross the placental trophoblast and effectively shield digoxin from P-gp efflux. Our hypothesis for this study was that endocytosis of nanoparticles would prevent digoxin from entering P-gp through the membrane and thus reduce the ability of P-gp to cause efflux of digoxin. Digoxin can still be effluxed from the cytosol by P-gp following its release out of the polymer matrix, but much more digoxin is able to cross the membrane without being effluxed. Thus, the amount of drug that is able to cross the basolateral membrane into the fetal circulation would be much higher. This effectively solves one of the crucial problems in fetal digoxin therapy by the

transplacental route, namely the inability of digoxin to reach the fetus in appreciable concentrations from the maternal circulation.

Synthesis and characterization of folic acid-functionalized nanoparticles loaded with digoxin

Though polymeric nanoparticles were able to overcome P-gp efflux by the placenta, these particles would still theoretically be available in the maternal circulation. Though maternal toxicity would likely be less, digoxin would still be present in the maternal circulation and may still cause maternal side effects. This is because these nanoparticles were non-targeted.

In order to delivery digoxin specifically to the fetal tissue transplacentally, we incorporated the idea of folate receptor-targeted nanoparticles. Folate receptor-mediated endocytosis is a well known phenomenon in many folate receptor-expressing cells. Many attempts at folate receptor targeting of nanoparticles in the past utilize chemotherapeutics for cancer therapy, as many carcinomas express folate receptors on their surface [78]. During pregnancy, placental trophoblast express relatively high folate receptor concentrations compared to the physiological expression of folate receptors in other tissues [79]. Thus, it is conceivable that folate receptor targeting can increase delivery of digoxin across the placenta into the fetal compartment. Due to high folate receptor expression in the placenta, timing of delivery should not have to coincide with optimized folate receptor expression levels; rather, these nanoparticles would be administered immediately following diagnosis of fetal tachyarrhythmia.

We attempted multiple synthesis techniques in order to prepare folate-functionalized PEG-PLGA. It was evident that increasing the availability of carboxylic acid groups on PLGA to react with the amine group of NH$_2$-PEG-Folate was critical in obtaining high conjugation to the polymers. We confirmed high conjugation of our

products by both GPC and folate absorbance at 405 nm. We also examined the thermal properties of the polymers that we synthesized, in various ratios with PLGA. It is evident that nanoprecipitation of PLGA with PLGA-PEG-Folate requires high ratios of PLGA-PEG-Folate in order to form homogenous polymer matrices and reduce separate crystallization of the two polymers.

Comparison of digoxin loaded folate-targeted and non-targeted nanoparticle transport in *in vitro* placental model

This chapter was designed to test the concept of targeted delivery of digoxin-loaded nanoparticles across the placenta to the fetus, the second step to improve digoxin therapy for fetal tachyarrhythmia. We successfully prepared digoxin-loaded folate-targeted nanoparticles for *in vitro* evaluation of their permeability across BeWo cells. This transport study showed that folate targeted digoxin-loaded nanoparticles could participate in folate receptor-mediated endocytosis to increase uptake of nanoparticles into and across placental trophoblast. The availability of folate receptors on the trophoblast surface were shown to be crucial in the endocytosis of these nanoparticles, as excess folate in the apical medium caused decreased transport of digoxin in folate-conjugated nanoparticles. Additionally, we provided another control testing the permeability of free digoxin in the presence of polymeric nanoparticles that had not been digoxin-loaded. Indeed, encapsulation of digoxin is necessary to increase its transplacental delivery.

We were also able to conjugate a near infrared fluorescent dye, DY-700, to PLGA and incorporate it into nanoprecipitated PLGA for imaging using an *in vivo* imaging system. The concentrations of dye that were detectable will allow us to determine an appropriate dose for *in vivo* imaging of folate-targeted nanoparticles in a pregnant rat model. In the future, we will be able to examine the biodistribution and fetal uptake of

these nanoparticles *in vivo*, informing the further development of these particles for clinical application.

Improving digoxin-loaded nanoformulations for fetal delivery

An important next step in the further development of these nanoformulations is to optimize the folate-targeting capability of these nanoparticles. While we show that folate-functionalized nanoparticles likely improve the transplacental permeability of digoxin, we do not know exactly what proportion of folic acid on the surface of nanoparticles will be optimal for transplacental delivery. It is possible that there could be a lower limit of folate-availability on the surface of nanoparticles, below which no observable difference is seen in transplacental transport. However, it could also be that after a certain point, high folate density could hinder the ability of folate to act as a ligand at the receptor. An investigation of the correlation between the proportion of folate available on the surface and transplacental permeability could be conducted as an optimization step for this nanoformulation strategy.

Ex vivo placental perfusions

Another study that could be conducted is the determination of the fetal transfer rate of digoxin in these nanoformulations using the *ex vivo* placental perfusion model. This is a well-studied and validated model of transplacental drug transport, and allows mechanistic studies of transport while mimicking the human pregnant patient. Placentas obtained immediately after delivery can be perfused with oxygenated medium to keep

them viable. Nanoformulations of digoxin can then be administered to the maternal circulation reservoir, and concentrations of digoxin can be detected in the fetal circulation. This model provides additional benefits of having more placental elements present, including the complex chorionic villous structure, fetal capillary endothelium, and villous stroma present. Tissue uptake, too, can be more adequately assessed by this approach. However, it is important to perform these studies using physiologically relevant pH, electrolyte, protein and drug concentrations. Radiolabeled digoxin, emitting beta radiation, could be used to quantify low concentrations of digoxin that would be used in these studies.

**In vivo studies and clinical trials**

Another possibility in the evaluation of these nanoparticles in pregnancy would be *in vivo* studies using pregnant rats. We have already been able to prepare fluorophore conjugated PLGA that is detectable in low concentrations by IVIS. Loading this fluorophore tagged polymer into folate-targeted nanoparticles in comparison to non-targeted polymer would allow us to examine the effect of folate-targeting on biodistribution of these nanoparticles during pregnancy.

Pregnant baboons can also be used as a predictive model mimicking human pregnancy. The placental structure and function of baboons is very similar to that of humans, and would give a more accurate prediction of the performance of folate-targeted nanoparticles in pregnancy. Unanticipated toxicity from these nanoparticles can also be evaluated before this formulation is administered to pregnant patients.

Clinical trials of these nanoparticles represent the final hurdle before these particles are available for use during pregnancy. Investigations of these nanoparticles in pregnancy, specifically their ability to reduce maternal side effects and improve fetal outcomes, will be necessary going forward.

Appendix A: Standard Curves

A.1. Standard curve for folic acid absorbance
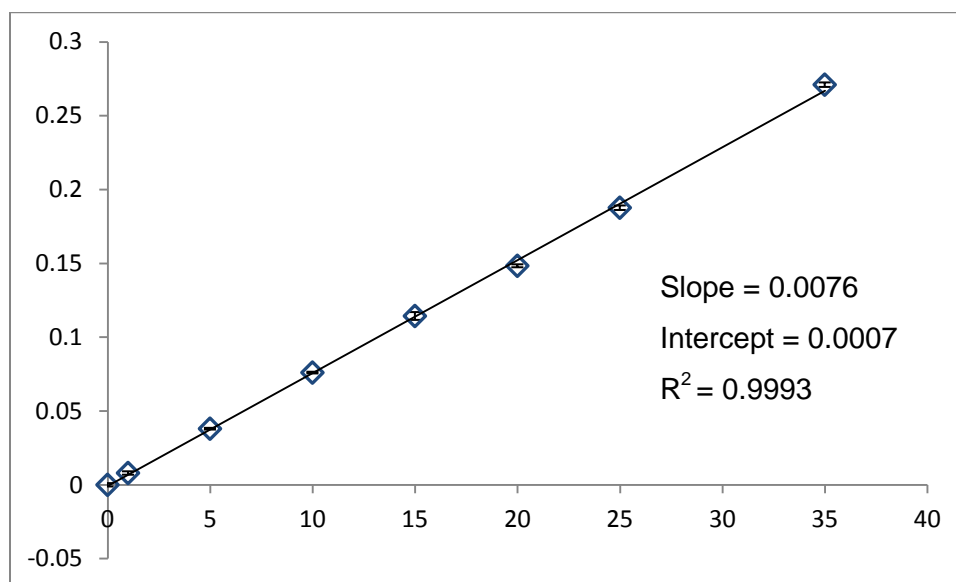
Folate absorbance was measured in DMSO at 365 nm by plate reader. Folate absorbance is linear from 1 to 35 µg/mL. All products were measured using a BioTek µQuant Plate Reader (Winooski, Vermont). Absorbance values are corrected for blank DMSO. Error bars indicate standard deviation of 3 samples.

A.2. Standard curve for gel permeation chromatography
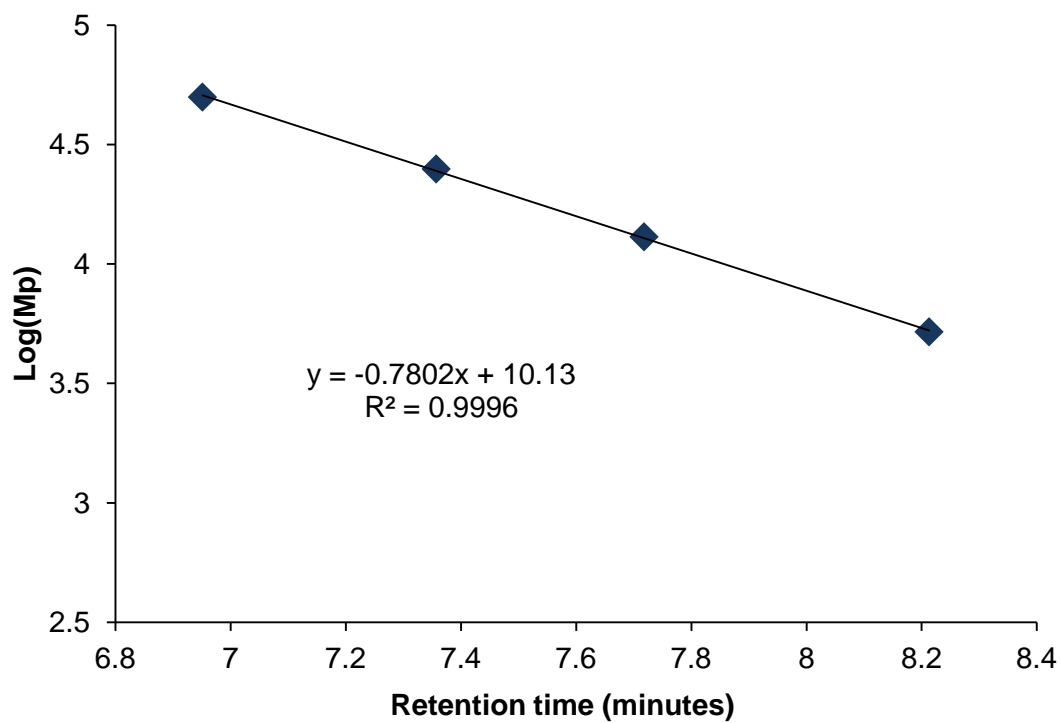
This curve plots $\log_{10}(M_p)$ vs. retention time for four polystyrene molecular weight standards (5.2, 13, 30, and 50 kDa).

A.3. Standard curve for digoxin detection in media by HPLC/PDA detector
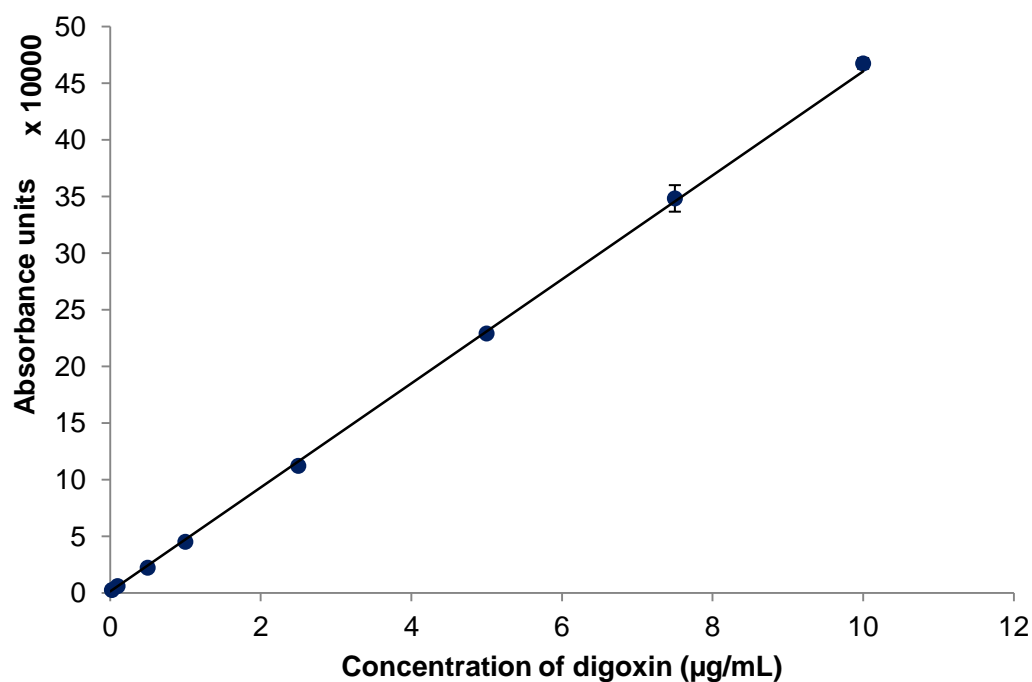
Standard curve of digoxin detection by HPLC/PDA detector was prepared using standards of digoxin dissolved in cell culture media (50:50 DMEM/F-12). Detection is linear, accurate, and precise across all required concentration ranges. Error bars indicate standard deviation of three injections.

A.4. Standard curve for DY-700 nanoparticle fluorescence
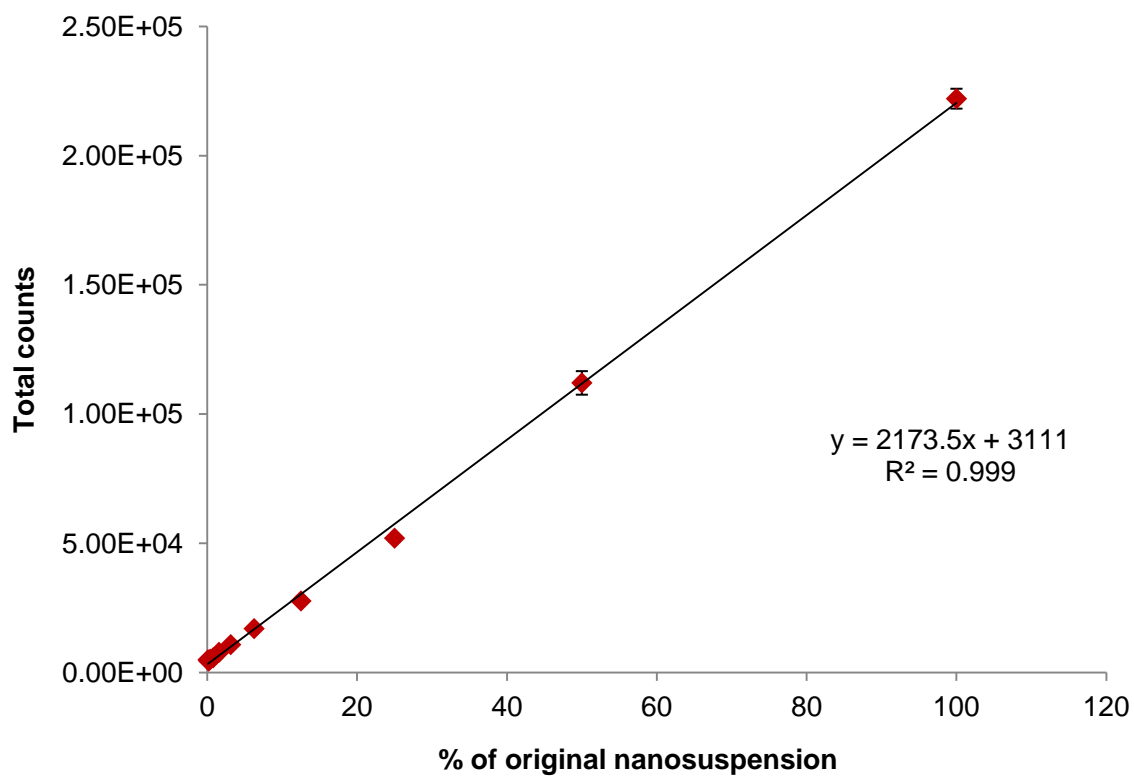
Detection of fluorescent nanoparticles is linear until 0.1% of the original nanosuspension, but background autofluorescence becomes an issue when detecting concentrations below 12.5% of the original nanosuspension concentration.

A.5. Apparent permeability values and relative standard deviations for folate-targeted nanoparticle transport study

Treatment group	Average P_e (cm/s)	StDev	%RSD
Free DG	3.66×10^{-6}	1.07×10^{-6}	29.2%
Free DG + blank NPs	8.03×10^{-6}	2.48×10^{-6}	72.7%
Non-targeted DG-NPs	1.25×10^{-5}	6.93×10^{-6}	75.5%
Folate DG-NPs	9.44×10^{-6}	1.86×10^{-6}	19.7%
Folate DG-NPs + excess folate	5.04×10^{-6}	1.36×10^{-6}	26.9%

References

(1)   Huhta, J. C. *Semin. Fetal & Neonatal Med.* **2005**, *10*, 542–552.

(2)   Thakur, V.; Fouron, J.-C.; Mertens, L.; Jaeggi, E. T. *Can. J. Cardiol.* **2013**, *29*, 759–767.

(3)   Sekarski, N.; Meijboom, E. J.; Di Bernardo, S.; Ksontini, T. B.; Mivelaz, Y. *Eur. J. Pediatr.* **2014**, *173*, 983–996.

(4)   Donofrio, M. T.; Moon-Grady, A. J.; Hornberger, L. K.; Copel, J. A.; Sklansky, M. S.; Abuhamad, A.; Cuneo, B. F.; Huhta, J. C.; Jonas, R. A.; Krishnan, A.; Lacey, S.; Lee, W.; Michelfelder, E. C.; Rempel, G. R.; Silverman, N. H.; Spray, T. L.; Strasburger, J. F.; Tworetzky, W.; Rychik, J.; Rychik. *Circulation* **2014**, *129*, 2183–2242.

(5)   Rana, Y. S.; Sodhi, B.; Kochar, S.; Arora, D. *J. South Asian Fed. Obstet. Gynaecol.* **2009**, *1*, 44–46.

(6)   Kleinman, C. S.; Nehgme, R. A. Cardiac Arrhythmias in the Human Fetus, 2004, *25*.

(7)   Parker, L. A. *Newborn Infant Nurs. Rev.* **2006**, *6*, e1–e8.

(8)   Hofstaetter, C.; Hansmann, M.; Eik-Nes, S. H.; Huhta, J. C.; Luther, S. L. *J. Matern. & Neonatal Med. : Off. J. Eur. Assoc. Perinat. Med. Fed. Asia Ocean. Perinat. Soc. Int. Soc. Perinat. Obstet.* **2006**, *19*, 407–413.

(9)   McElhinney, D. B.; Tworetzky, W.; Lock, J. E. *Circulation* **2010**, *121*, 1256–1263.

(10)   Suri, V.; Keepanaseril, A.; Aggarwal, N.; Vijayvergiya, R. *Indian J. Med. Sci.* **2009**, *63*, 411–414.

(11)   Heerdt, P. M.; Heerdt, M. E. *J. Clin. Anesth.* **1992**, *4*, 419–435.

(12)   Xia, B.; Heimbach, T.; Gollen, R.; Nanavati, C.; He, H. *AAPS J.* **2013**, *15*, 1012–1024.

(13)   Lelievre, L. G.; Lechat, P. *Heart Metab* **2007**, *35*.

(14)   Ehle, M.; Patel, C.; Giugliano, R. P. *Crit. pathways Cardiol.* **2011**, *10*, 93–98.

(15)   Gheorghiade, M.; van Veldhuisen, D. J.; Colucci, W. S. *Circulation* **2006**, *113*, 2556–2564.

(16)   Azancot-Benisty, A.; Jacqz-Aigrain, E.; Guirgis, N. M.; Decrepy, A.; Oury, J. F.; Blot, P. *J. Pediatr.* **1992**, *121*, 608–613.

(17)   Rytting, E.; Ahmed, M. S. 5 - Fetal Drug Therapy. *Clinical Pharmacology During Pregnancy*, 2013, 55–72.

(18)   Ward, R. M. Pharmacology of the maternal-placental-fetal-unit and fetal therapy. *Progress in Pediatric Cardiology*, 1996, *5*, 79–89.

(19)   Singh, Y.; Sodhi, B.; Kochar, S. P. S.; Arora, D. *J. South Asian Fed. Obstet. Gynecol.* **2009**, *1*, 44–46.

(20)   Miller, R. K. *Clin. Obstet. Gynecol.* **1991**, *34*, 241–250.

(21)   Evans, M. I.; Pryde, P. G.; Reichler, A.; Bardicef, M.; Johnson, M. P. *West. J. Med.* **1993**, *159*, 325–332.

(22)   Frishman, W. H.; Elkayam, U.; Aronow, W. S. *Cardiol. Clin.* **2012**, *30*, 463–491.

(23)   Hebert, M. F.; Easterling, T. R.; Kirby, B.; Carr, D. B.; Buchanan, M. L.; Rutherford, T.; Thummel, K. E.; Fishbein, D. P.; Unadkat, J. D. *Clin. Pharmacol. Ther.* **2008**, *84*, 248–253.

(24)   Okada, R. D.; Hager, W. D.; Graves, P. E.; Mayersohn, M.; Perrier, D. G.; Marcus, F. I. *Circulation* **1978**, *58*, 1196–1203.

(25)   Carter, A. M. *Physiol. Rev.* **2012**, *92*, 1543–1576.

(26)   Poulsen, M. S.; Rytting, E.; Mose, T.; Knudsen, L. E. *Toxicol. Vitr. : Int. J. Publ. Assoc. with BIBRA* **2009**, *23*, 1380–1386.

(27)   Dewhurst's Textbook of Obstetrics & Gynaecology, Eighth Edition - Wiley Online Library, 2015.

(28)   Du, X.; Yuan, Q.; Yao, Y.; Li, Z.; Zhang, H. *Int. J. Clin. Exp. Med.* **2014**, *7*, 4660–4665.

(29)   Goebelsmann, U. *J. Reprod. Med.* **1979**, *23*, 166–177.

(30)   Hemauer, S. J.; Nanovskaya, T. N.; Abdel-Rahman, S. Z.; Patrikeeva, S. L.; Hankins, G. D. V.; Ahmed, M. S. *Biochem. Pharmacol.* **2010**, *79*, 921–925.

(31)   Hemauer, S. J.; Patrikeeva, S. L.; Nanovskaya, T. N.; Hankins, G. D. V.; Ahmed, M. S. *Am. J. Obstet. Gynecol.* **2010**, *202*, 383.e1–e383.e7.

(32)   Stapleton, P. A.; Nurkiewicz, T. R. *Nanomedicine* **2014**, *9*, 929–931.

(33)   Ema, M.; Kobayashi, N.; Naya, M.; Hanai, S.; Nakanishi, J. *Reprod. Toxicol.* **2010**, *30*, 343–352.

(34)   Yang, Y.; Westerhoff, P. *Adv. Exp. Med. Biol.* **2014**, *811*, 1–17.

(35)   Ali, S.; Rytting, E. *Adv. Exp. Med. Biol.* **2014**, *811*, 45–54.

(36)   Shimizu, M.; Tainaka, H.; Oba, T.; Mizuo, K.; Umezawa, M.; Takeda, K. *Part.*

Fibre Toxicol. **2009**, *6*.

(37) Fedulov, A. V.; Leme, A.; Yang, Z.; Dahl, M.; Lim, R.; Mariani, T. J.; Kobzik, L. *Am. J. Respir. cell Mol. Biol.* **2008**, *38*, 57–67.

(38) Takeda, K.; Suzuki, K.; Ishihara, A.; Kubo-Irie, M.; Fujimoto, R.; Tabata, M.; Oshio, S.; Nihei, Y.; Ihara, T.; Sugamata, M. *J. Health Sci.* **2009**, *55*, 95–102.

(39) Danhier, F.; Ansorena, E.; Silva, J. M.; Coco, R.; Le Breton, A.; Préat, V. *J. Control. Release : Off. J. Control. Release Soc.* **2012**, *161*, 505–522.

(40) Wang, J.; Wang, M.; Zheng, M.; Guo, Q.; Wang, Y.; Wang, H.; Xie, X.; Huang, F.; Gong, R. *Colloids surfaces. B, Biointerfaces* **2015**, *129*, 63–70.

(41) Williams, P. J.; Bulmer, J. N.; Innes, B. A.; Broughton Pipkin, F. *Biol. Reprod.* **2011**, *84*, 1148–1153.

(42) Albekairi, N. A.; Rytting, E. *CRS Newsl.* **2014**, 10–11.

(43) Rosenberg, A. A.; Galan, H. L. *Pediatr. Clin. North Am.* **1997**, *44*, 113–135.

(44) Mongiovì, M.; Fesslova, V.; Fazio, G.; Barbaro, G.; Pipitone, S. *Curr. Pharm. Des.* **2010**, *16*, 2929–2934.

(45) Petropoulos, S.; Gibb, W.; Matthews, S. G. *Brain Res.* **2010**, *1357*, 9–18.

(46) Utoguchi, N.; Chandorkar, G. A.; Avery, M.; Audus, K. L. *Reprod. Toxicol.* **2000**, *14*, 217–224.

(47) Cartwright, L.; Poulsen, M. S.; Nielsen, H. M.; Pojana, G.; Knudsen, L. E.; Saunders, M.; Rytting, E. *Int. J. nanomedicine* **2012**, *7*, 497–510.

(48) Makadia, H. K.; Siegel, S. J. *Polymers* **2011**, *3*, 1377–1397.

(49) Campolongo, M. J.; Luo, D. *Nat. Mater.* **2009**, *8*, 447–448.

(50) Hemauer, S. J.; Patrikeeva, S. L.; Nanovskaya, T. N.; Hankins, G. D. V.; Ahmed, M. S. *Biochem. Pharmacol.* **2009**, *78*, 1272–1278.

(51) Beck-Broichsitter, M.; Rytting, E.; Lebhardt, T.; Wang, X.; Kissel, T. *Eur. J. Pharm. Sci. : Off. J. Eur. Fed. Pharm. Sci.* **2010**, *41*, 244–253.

(52) Rytting, E.; Bur, M.; Cartier, R.; Bouyssou, T.; Wang, X.; Krüger, M.; Lehr, C.-M.; Kissel, T. *J. Control. Release : Off. J. Control. Release Soc.* **2010**, *141*, 101–107.

(53) Ali, H.; Kalashnikova, I.; White, M. A.; Sherman, M.; Rytting, E. *Int. J. Pharm.* **2013**, *454*, 149–157.

(54) Ali, H.; Kilic, G.; Vincent, K.; Motamedi, M.; Rytting, E. *Ther. Deliv.* **2013**, *4*, 161–175.

(55)   Ushigome, F.; Takanaga, H.; Matsuo, H.; Yanai, S.; Tsukimori, K.; Nakano, H.;
        Uchiumi, T.; Nakamura, T.; Kuwano, M.; Ohtani, H.; Sawada, Y. *Eur. J.
        Pharmacol.* **2000**, *408*, 1–10.

(56)   Bode, C. J.; Jin, H.; Rytting, E.; Silverstein, P. S.; Young, A. M.; Audus, K. L.
        Methods Mol. Med. **2006**, *122*, 225–239.

(57)   Huang, Q.; Li, J.; Wang, F.; Oliver, M. T.; Tipton, T.; Gao, Y.; Jiang, S.-W. *Cell.
        Signal.* **2013**, *25*, 1027–1035.

(58)   Mørck, T. J.; Sorda, G.; Bechi, N.; Rasmussen, B. S.; Nielsen, J. B.; Ietta, F.;
        Rytting, E.; Mathiesen, L.; Paulesu, L.; Knudsen, L. E. *Reprod. Toxicol.* **2010**, *30*,
        131–137.

(59)   Vande Vannet, B. M. R. A.; Hanssens, J. L. *Angle Orthod.* **2007**, *77*, 716–722.

(60)   Huang, Y.; Dai, W.-G. *Acta Pharm. Sin. B* **2014**, *4*, 18–25.

(61)   Siepmann, J.; Peppas, N. A. *Int. J. Pharm.* **2011**, *418*, 6–12.

(62)   Siepmann, J.; Peppas, N. A. *Adv. drug Deliv. Rev.* **2001**, *48*, 139–157.

(63)   Wick, P.; Malek, A.; Manser, P.; Meili, D.; Maeder-Althaus, X.; Diener, L.;
        Diener, P.-A.; Zisch, A.; Krug, H. F.; von Mandach, U. *Environ. Health Perspect.*
        2010, *118*, 432–436.

(64)   Rytting, E.; Nguyen, J.; Wang, X.; Kissel, T. *Expert Opin. drug Deliv.* **2008**, *5*,
        629–639.

(65)   Iversen, T.-G.; Skotland, T.; Sandvig, K. *Nano Today* **2011**, *6*, 176–185.

(66)   Herd, H.; Daum, N.; Jones, A. T.; Huwer, H.; Ghandehari, H.; Lehr, C.-M. *ACS
        nano* **2013**, *7*, 1961–1973.

(67)   Leamon, C. P.; Jackman, A. L. *Vitam. Horm.* **2008**, *79*, 203–233.

(68)   Prasad, P. D.; Ramamoorthy, S.; Moe, A. J.; Smith, C. H.; Leibach, F. H.;
        Ganapathy, V. *Biochim. et Biophys. Acta* **1994**, *1223*, 71–75.

(69)   Antony, A. C. *Annu. Rev. Nutr.* **1996**, *16*, 501–521.

(70)   Yoo, H. S.; Park, T. G. *J. Control. Release : Off. J. Control. Release Soc.* **2004**,
        96, 273–283.

(71)   Esmaeili, F.; Ghahremani, M. H.; Ostad, S. N.; Atyabi, F.; Seyedabadi, M.;
        Malekshahi, M. R.; Amini, M.; Dinarvand, R. *J. drug Target.* **2008**, *16*, 415–423.

(72)   Yoo, H. S.; Park, T. G. *J. Control. Release : Off. J. Control. Release Soc.* **2004**,
        100, 247–256.

(73)   Pannu, R. K.; Tanodekaew, S.; Li, W.; Collett, J. H.; Attwood, D.; Booth, C.

Biomaterials **1999**, *20*, 1381–1387.

(74)   Dudowicz, J.; Douglas, J. F.; Freed, K. F. *J. Chem. Phys.* **2014**, *140*.

(75)   Yasuda, S.; Hasui, S.; Kobayashi, M.; Itagaki, S.; Hirano, T.; Iseki, K. *Biosci. Biotechnol. Biochem.* **2008**, *72*, 329–334.

(76)   Nicolas, J.; Tsapis, N.; Reul, R.; Recher, M.; Fattal, E.; Hillaireau, H.; Mura, S.; Coll, J.-L.; Sancey, L. *Polym. Chem.* **2012**, *3*, 694–702.

(77)   McNulty, B.; McNulty, H.; Marshall, B.; Ward, M.; Molloy, A. M.; Scott, J. M.; Dornan, J.; Pentieva, K. *Am. J. Clin. Nutr.* **2013**, *98*, 92–98.

(78)   Parker, N.; Turk, M. J.; Westrick, E.; Lewis, J. D.; Low, P. S.; Leamon, C. P. *Anal. Biochem.* **2005**, *338*, 284–293.

(79)   Ross, J. F.; Chaudhuri, P. K.; Ratnam, M. *Cancer* **1994**, *73*, 2432–2443.